

Accepted Manuscript

Reduced-complexity probabilistic reconstruction of alluvial aquifer stratigraphy, and application to sedimentary fans in northwestern India

Wout M. van Dijk, Alexander L. Densmore, Rajiv Sinha, Ajit Singh, Vaughan R. Voller

PII: S0022-1694(16)30518-2

DOI: <http://dx.doi.org/10.1016/j.jhydrol.2016.08.028>

Reference: HYDROL 21463

To appear in: *Journal of Hydrology*

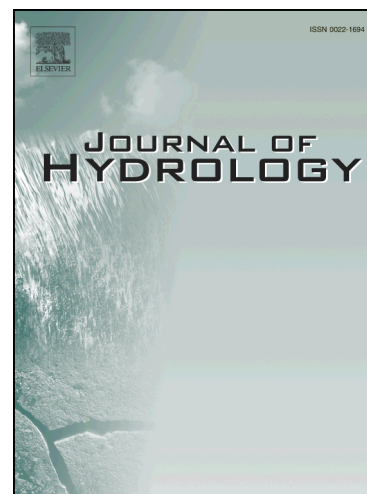
Received Date: 1 March 2016

Revised Date: 8 August 2016

Accepted Date: 15 August 2016

Please cite this article as: van Dijk, W.M., Densmore, A.L., Sinha, R., Singh, A., Voller, V.R., Reduced-complexity probabilistic reconstruction of alluvial aquifer stratigraphy, and application to sedimentary fans in northwestern India, *Journal of Hydrology* (2016), doi: <http://dx.doi.org/10.1016/j.jhydrol.2016.08.028>

This is a PDF file of an unedited manuscript that has been accepted for publication. As a service to our customers we are providing this early version of the manuscript. The manuscript will undergo copyediting, typesetting, and review of the resulting proof before it is published in its final form. Please note that during the production process errors may be discovered which could affect the content, and all legal disclaimers that apply to the journal pertain.



Reduced-complexity probabilistic reconstruction of alluvial aquifer stratigraphy, and application to sedimentary fans in northwestern India

Wout M. van Dijk^{a,b,*}, Alexander L. Densmore^a, Rajiv Sinha^c, Ajit Singh^d,
Vaughan R. Voller^e

^a*Department of Geography, Durham University, Durham, UK.*

^b*Faculty of Geosciences, Universiteit Utrecht, Utrecht, The Netherlands*

^c*Department of Earth Sciences, Indian Institute of Technology Kanpur, Kanpur, India.*

^d*Faculty of Engineering, Department of Earth Science & Engineering, Imperial College, London, UK.*

^e*Department of Civil, Environmental, and Geo-Engineering, National Center for Earth Surface Dynamics, Saint Anthony Falls Laboratory, University of Minnesota, Twin Cities, Minneapolis, Minnesota, USA.*

Abstract

Generating a realistic model of subsurface stratigraphy that fits data from multiple well locations is a well-established problem in the field of aquifer characterization. This is particularly critical for the alluvial fan-hosted aquifers in northwestern India, as they have some of the highest rates of groundwater extraction in the world and spatially limited subsurface observations. The objective of this study is to develop a reduced-complexity model that generates probabilistic estimates of aquifer body occurrence within a sedimentary fan, based loosely on the northwestern Indian aquifer system. We propose a parsimonious, inverse-weighted random walk model that reconstructs potential channel belt pathways within a discrete depth range or slice by (i) connecting known aquifer locations

*Corresponding author

Email address: woutvandijk@gmail.com (Wout M. van Dijk)

with the fan apex, (ii) filling adjacent cells with non-aquifer material based on estimated channel-body dimensions, and (iii) random filling of the remaining cells until the model fraction of aquifer material is comparable to the bulk aquifer fraction observed from well data. Once filled, individual depth slices can be stacked to produce a three-dimensional representation of aquifer-body geometry, allowing informed inference and testable predictions about the configuration of aquifer units in the subsurface. A receiver operating characteristic (ROC) curve shows that the model performs better than fully random filling, both in matching the locations of aquifer material in the subsurface and in reconstructing the geometry of relict channel bodies preserved on the fan surface. The model differs from purely statistical-empirical approaches by incorporating some geomorphic knowledge of fluvial channel belt geometry within the fan system. In contrast to a fully process-based approach, the model is computationally fast and is easily refined as new subsurface data become available.

Keywords: Numerical model, alluvial aquifers, aquifer-body connectivity, fan system

1 **1. Introduction**

2 Reconstruction of subsurface stratigraphy based on spatially-limited borehole
3 data is a well-established problem in the field of aquifer characterization. This re-
4 construction is particularly challenging for alluvial aquifer systems that consist of
5 fluvial channel deposits, in which the major aquifer units comprise stacked sand-
6 rich channel belts associated with alluvial fans or meandering river channels. Such
7 settings are marked by high subsurface heterogeneity in aquifer-body characteris-
8 tics and distribution due to frequent avulsion and migration of the active channel

9 during deposition. Information derived from geophysical profiles, cores, well logs
10 and well-test data is rarely sufficient (due to limited spatial coverage) to determine
11 the three-dimensional geometry, size, and connectivity of aquifer bodies within
12 these settings. These aspects of the system are critical, however, because they
13 control aquifer volume, potential yield, and flow rates, and thus both aquifer per-
14 formance and sustainability (Larue and Hovadik, 2006; Renard and Allard, 2013).
15 Connectivity in particular is related to the existence of pathways between aquifer
16 bodies that enable fast flow and transport from one location to another (Renard
17 and Allard, 2013). There is a pressing need for simple, flexible, and predictable
18 models that can simulate or anticipate these pathways. The paucity of subsurface
19 data in many alluvial aquifer systems, and the predominance of elongate channel-
20 body aquifers, preclude simple lateral correlation between aquifer bodies recorded
21 in different wells, while the lack of detailed lithological data, including age con-
22 straints, may preclude the use of more sophisticated forward models that could
23 simulate aquifer-system deposition and development.

24 Previous approaches to this problem can be divided into structure-imitating,
25 process-imitating, and descriptive methods (Koltermann and Gorelick, 1996; de Marsily
26 et al., 2005). Structure-imitating methods, including spatial statistical and object-
27 based methods, rely on spatial patterns in sediments and hydraulic properties,
28 probabilistic rules, and deterministic constraints based on geometric relations within
29 aquifers (Koltermann and Gorelick, 1996). Statistical structure-imitating methods
30 include traditional two-point kriging or conditional methods (e.g., Isaak and Sri-
31 vastava, 1990; Journel, 1988) and modern multi-point statistical (MPS) methods
32 (e.g., Guardiano and Srivastava, 1993; Caers, 2001; Strebelle, 2002; Wu et al.,
33 2008; Comunian et al., 2012; Rezaee et al., 2013; Mariethoz and Lefebvre, 2014).

34 MPS methods offer a way to model complex and heterogeneous geological envi-
35 ronments through the use of training images, which represent conceptual statisti-
36 cal models of the geology that has to be simulated. While MPS methods are able to
37 describe richer and arguably more realistic models than two-point methods, they
38 have several shortcomings (Wingate et al., 2015): MPS is a purely statistical ap-
39 proach and requires suitable training images, which may provide model outcomes
40 that are statistically plausible but physically unrealistic. In contrast, object-based
41 methods use geometric or probabilistic rules, such as random walk approaches
42 (Price, 1974) or random avulsions (Jerolmack and Paola, 2007), to mimic deposi-
43 tional facies seen in nature (Koltermann and Gorelick, 1996). A geological record
44 is simulated either through rules-based on conceptual depositional models and
45 geologic principles, or through initial conditions, boundary conditions, and inputs
46 such as sea level curves, subsidence histories, and sediment supplies (See review
47 in Koltermann and Gorelick, 1996).

48 Process-imitating methods (e.g., Karssenberg et al., 2001; Pyrcz et al., 2005;
49 Sylvester et al., 2011; Nicholas et al., 2016; Van de Lageweg et al., 2016a) are
50 algorithms that solve a set of governing equations that mimic the processes of
51 sediment transport and deposition in sedimentary basins and build stratigraphy
52 (Koltermann and Gorelick, 1996). In contrast to structure-imitating methods,
53 process-imitating methods simulate physical processes and therefore have the po-
54 tential to predict realistic subsurface geometries and distributions of channel-belt
55 sand bodies (Mackey and Bridge, 1995). In process-based models, the deposi-
56 tional surface is updated at each time step under the influence of both depositional
57 and erosional processes. This makes it difficult to condition the outcome with
58 observed data (Karssenberg et al., 2001; Wingate et al., 2015), because initial de-

59 posits may fit the data but are later erased. In addition, full fluid-dynamical sim-
60 ulations are too slow for simulating long-term basin development, as they use too
61 much computational power to iteratively fit observed data. An important draw-
62 back of even simplified process-imitating models is that they still need several
63 parameters, which may or may not be either physically-based or independently
64 known. Also, process-based models ideally require quantitative stratigraphic in-
65 formation, including depositional ages and subsidence rates, in order to make
66 systematic comparisons between model outputs and real systems.

67 Descriptive methods produce images of subsurface stratigraphy by combining
68 site-specific and regional data with conceptual models (e.g., Allen, 1978; Gal-
69 loway, 1981; Miall, 1985; Nemeč and Steel, 1988) and insights (Koltermann and
70 Gorelick, 1996; Van de Lageweg et al., 2016b). Descriptive methods split the
71 aquifer into characteristic units that are based equally on hydraulic measurements
72 and geologic observations (Fogg, 1986; Anderson, 1989). Characteristic units for
73 reconstructing aquifer corridors are often based on the distinction between hetero-
74 geneous fluvial deposits such as gravel or sand-rich channel deposits (assumed to
75 be aquifer material) and silt or clay-rich floodplain deposits (assumed to be non-
76 aquifer material) (Miall, 1988; Jordan and Pryor, 1992; Willis and Tang, 2010).

77 In the field of fluvial routing systems, e.g., fans and deltas, hybrid models
78 combining elements of structure-imitating and process-imitating approaches have
79 also been successfully applied to reconstruct the depositional fan settings. For ex-
80 ample, several studies have recognized the connection between avulsion processes
81 in fluvial sediment routing systems and the stratigraphy of channel sand bodies in
82 the field (e.g., Price, 1974; Leeder, 1978; Allen, 1979; Bridge and Leeder, 1979;
83 Bridge and Mackey, 1993). Thus, avulsion processes have been included, partly

84 as probabilistic rules, in several reduced-complexity models (e.g., Price, 1974;
85 Mackey and Bridge, 1995; Karssenberget al., 2001; Jerolmack and Paola, 2007;
86 Liang et al., 2015a). Such models have been used to reconstruct channel-belt
87 deposits from the apex of the system to downstream locations based on a ran-
88 dom walk, the local gradient and an avulsion probability that is dependent upon
89 sediment input and changes in base level. Even these simplistic rules can pro-
90 duce flow velocities and water surface slopes (Liang et al., 2015b) and subsurface
91 stratigraphic records (Karssenberget al., 2001; Jerolmack and Paola, 2007; Liang
92 et al., 2015b) that are comparable to the outputs of more sophisticated process-
93 based models of fluvial routing systems. These fan models are, however, rarely
94 used to reconstruct fan deposits from actual well log information.

95 Robust reconstruction of subsurface stratigraphy has major implications for
96 our understanding of the aquifer system in northwestern India, which suffers from
97 some of the highest rates of groundwater over-exploitation and water-level decline
98 in the world (Rodell et al., 2009; Chen et al., 2014, 2016). Accurate geological
99 characterisation of the aquifer system has been hampered by a lack of subsurface
100 data; even basic first-order knowledge of aquifer-body dimensions and subsurface
101 distribution is lacking at a regional scale. Van Dijk et al. (2016) identified two ma-
102 jor fan systems in the region, and provided a descriptive conceptual model for the
103 aquifer bodies that inferred the likely aquifer distribution based on some well log
104 information and our understanding of fan systems. This conceptual model is insuf-
105 ficiently detailed, however, to populate local or regional hydrogeological models,
106 and provides only statistical descriptions of the full three-dimensional stratigra-
107 phy. Because of the size of the region (44,000 km²) and the spatial variation in
108 aquifer body fraction (Van Dijk et al., 2016) there is no suitable geological model

109 or three-dimensional training image that could inform a pure statistical structure-
110 imitating approach. The study area is also so large that conditioning of the data is
111 difficult and time-consuming, and the lack of suitable constraints on stratigraphic
112 geometry and age control make it difficult to apply process-imitating models.

113 Here we propose a physically-based heuristic model that predicts the potential
114 aquifer body distribution through incorporating our best process understanding of
115 how the aquifer system forms into a reduced-complexity model. Our approach
116 occupies the 'middle ground' identified by (Liang et al., 2015b) between detailed
117 and physically-explicit simulation on the one hand and abstract simplification on
118 the other. The model is based on the deposition of continuous sandy channel ma-
119 terial within the sediment fans that comprise the major aquifer systems in north-
120 western India, but we do not explicitly simulate channel transport and depositional
121 processes. Instead, we use geological and geomorphological information on the
122 downstream continuity and lateral discontinuity of the channel bodies, combined
123 with a random-walk approach, to reconstruct the most likely aquifer locations in a
124 given depth slice. We then show how two-dimensional sediment routing assump-
125 tions in a given depth slice can be used to build a three-dimensional picture of the
126 subsurface stratigraphy. We compare model predictions of aquifer-body positions
127 and connectivity to the null case of random filling of the basin, and consider the
128 implications of the model for groundwater exploration and management.

129 **2. Study Area**

130 The study area comprises the sediment fans deposited by the Sutlej and Ya-
131 muna Rivers within the Himalayan foreland basin. The area is bounded by the
132 Himalaya to the north, the Thar Desert to the south, and the incised valleys of

133 the Sutlej and Yamuna to the west and east, respectively (Figure 1). At present,
134 sediment flux into the foreland is dominated by the Sutlej and Yamuna Rivers, as
135 well as by smaller, foothills-fed and plains-fed river systems such as the Ghaggar
136 River (Van Dijk et al., 2016).

137 Available data on aquifer-body thickness and location consist of 243 aquifer-
138 thickness logs from the Central Groundwater Board (CGWB). These logs make a
139 binary division of the subsurface into aquifer and non-aquifer units, and provide
140 the depth and thickness of each layer as estimated from electrical logs by the
141 CGWB. The logs have a median spacing of 7 km (Van Dijk et al., 2016). All of
142 the logs extend to at least 200 m below ground level, and we therefore restrict our
143 analysis to the top 200 m of the subsurface, noting that there is no evidence that
144 aquifers deeper than 200 m have yet been tapped in this region.

145 Van Dijk et al. (2016) mapped different geomorphic units and showed a di-
146 rect correlation between these units and the bulk characteristics of the underlying
147 aquifer bodies (Figure 1). Van Dijk et al. (2016) showed that, across the Sutlej
148 and Yamuna sedimentary fan systems, individual aquifer bodies have a median
149 thickness of 6-7 m and a mean thickness of 9 m. The aquifer-body thickness dis-
150 tributions are heavy-tailed (Van Dijk et al., 2016), indicating that there is some
151 persistence in aquifer location. Over larger stratigraphic intervals of more than
152 4-8 times the median thickness, the aquifer thickness logs show evidence of im-
153 persistence, perhaps related to avulsion and compensational filling. Van Dijk et al.
154 (2016) inferred that the thicker aquifer deposits are formed by stacked, multi-story
155 sand bodies, perhaps originating in part as incised-valley fills, that occupied dis-
156 tinct corridors originating at the fan apices. Van Dijk et al. (2016) were unable to
157 directly observe the widths of these corridors, but inferred a maximum width of

158 5-10 km by analogy with surface channel-belt widths (Van Dijk et al., 2016) and
159 thickness-width relations of Gibling (2006). The bulk aquifer fraction (f_{obs}), or
160 ratio between aquifer and non-aquifer material, is about 0.4 for both fan systems.
161 A major exception to this occurs in the area between the Sutlej and Yamuna fans
162 and adjacent to the Himalayan mountain front; there, aquifer bodies are both thin-
163 ner and less abundant, and the bulk aquifer fraction (f_{obs}) is about 0.3. Van Dijk
164 et al. (2016) also showed that the aquifer-body thickness distribution does not
165 change significantly with depth, which suggests that the morphodynamics and de-
166 positional conditions of the Sutlej and Yamuna sediment routing systems have
167 remained consistent over the time required to deposit at least the upper 200 m of
168 the subsurface stratigraphy. The bulk aquifer fraction decreases away from the
169 Himalayan mountain front in both the Sutlej and Yamuna fan systems, although
170 the thickness distribution remains approximately similar, indicating that aquifer
171 bodies make up a smaller fraction of the basin fill in the distal parts of the system
172 but do not thin appreciably.

173 **3. Model approach**

174 Our modelling approach builds on the aquifer-thickness logs from the CGWB,
175 which provide information on the presence or absence of aquifer material in the
176 upper 200 m at 243 points across the basin. We assume that the aquifer bodies
177 in the fan system were mainly deposited by major river channels that avulsed re-
178 peatedly across the fan surface during deposition. The likely maximum lateral
179 dimensions of the aquifer bodies (less than 5-10 km, Table 1) are comparable to
180 or smaller than the median spacing between adjacent logs (7 km), and Van Dijk
181 et al. (2016) showed the difficulty of correlating between even closely-spaced

182 boreholes, meaning that simple lateral (across-fan) extrapolation would be un-
183 wise. Similarly, while the river channels are continuous down-fan, channel-belt
184 sinuosity precludes simple longitudinal correlation or extrapolation as well. For
185 simplicity, we do not simulate the formation and filling of incised valleys in our
186 model; while this is a plausible mechanism for the creation of stacked aquifer
187 bodies like those observed in the study area, we have no data on its relative impor-
188 tance, and we note that its inclusion would require more complex process-based
189 approach.

190 To estimate the likelihood of finding aquifer material within a given depth
191 range between our borehole locations, we define a model space and apply a set
192 of simple rules derived from our geomorphic understanding of fan depositional
193 systems, including aspects such as avulsion sequence (Allen, 1978; Jerolmack
194 and Paola, 2007), compensational filling (Sheets et al., 2002; Straub et al., 2009),
195 and reoccupation (Stouthamer, 2005). We start by dividing the study area into
196 a regular, square grid, with a cell size that is chosen to reflect the typical lateral
197 dimensions of the aquifer bodies. This choice introduces an inherent length scale
198 into the model, but is made explicitly for two reasons. First, the large median
199 spacing between the aquifer-thickness logs means that there is no justification for
200 a fine model grid size, as there are no data against which to validate it. Second, a
201 relatively coarse grid obviates the need to model progressive deposition and con-
202 struction of sand bodies, as would be required by a process-imitating approach.
203 We then divide the upper 200 m of stratigraphy into regular depth slices and op-
204 erate on each slice in turn. The thickness of the depth slice is chosen to be of the
205 same order as both the median aquifer-body thickness of 6 m (Table 2) and the
206 median non-aquifer unit thickness of 7.5 m. Each slice is parallel to the present

207 topography, meaning that we assume that the modern basin surface slope is the
208 same as the slope throughout deposition. We neglect the local surface relief, as
209 this is typically less than 5 m, and assume that deposits at a given depth are ap-
210 proximately coeval. We explore the sensitivity of the model results to changes in
211 both grid size and depth slice thickness.

212 The model carries out five basic operations on each depth slice: (i) identify-
213 ing grid cells that contain dominantly aquifer or non-aquifer material, and filling
214 them appropriately; (ii) establishing upstream weighted random walks between
215 aquifer cells and the fan apex, and filling cells along those routes with aquifer
216 material; (iii) establishing downstream weighted random walks to define aquifer
217 corridors in both directions; (iv) filling cells adjacent to the aquifer corridors with
218 non-aquifer material; and (v) filling the remaining empty cells randomly up to the
219 correct bulk aquifer fraction (Figures 2b and c). These steps are then indepen-
220 dently repeated for successive depth slices. We then ran multiple realizations of
221 the model, and averaged the values in each cell to obtain probabilities of finding
222 aquifer bodies in the subsurface.

223 *3.1. Model setup*

224 The first underpinning assumption within the model is that thick channel sands
225 within a fan must have been deposited by a major river that entered the foreland
226 at the fan apex, rather than by smaller foothills-fed and plains-fed river systems
227 or reworking of fan material. This assumption is supported by the stacked, multi-
228 story character of the aquifer bodies and by their thickness (median 6 m), which is
229 much greater than the channel dimensions of smaller foothills-fed rivers like the
230 Ghaggar River (Sinha et al., 2013; Van Dijk et al., 2016), and by provenance data
231 that show that major channel sediments originate from the Himalayan hinterland

232 (Singh et al., 2016). The fan apices in our study area mark the points where
233 the Sutlej and Yamuna Rivers cross the Himalayan Frontal Thrust and enter the
234 foreland. While these points may shift over Myr time scales (e.g., Gupta, 1997;
235 Malik and Mohanty, 2007), we assume that they have remained fixed in space
236 over time needed to deposit the upper 200 m of sediment in the foreland basin.

237 Because of the fixed position of the rivers entering the basin and the relatively
238 thick sand bodies associated with these large river systems, we also assume that
239 aquifer material is continuous within each depth slice between its occurrence at
240 a point on the fan (as indicated by its appearance in the aquifer-thickness logs)
241 and the fan apex, although not necessarily in a straight line. We then use a ran-
242 dom walk approach to construct probable aquifer corridors in the upstream and
243 downstream directions from those wells that contain aquifer material in that depth
244 slice. The random walk is applied on a 2D plane, and represents the distribution
245 of aquifer bodies within that depth slice. For simplicity, we assume that aquifer
246 material, once deposited, is not scoured and replaced by non-aquifer deposits; we
247 justify this by noting the evidence for stacking and persistence in channel posi-
248 tions over stratigraphic intervals of 4-8 times the median aquifer-body thickness
249 (Van Dijk et al., 2016). The modelled aquifer body is, therefore, a continuous
250 channel deposit that is connected in both the upstream and downstream directions.

251 To avoid unreasonably straight channels, we set the weights in the upstream
252 random walk, toward the fan apex. We apply unequal weights justified by the
253 observed sinuosity of the modern Sutlej and Yamuna Rivers channel belts and
254 of elongate, sand-rich ridges on the fan surfaces, interpreted as abandoned river
255 palaeochannels by Van Dijk et al. (2016) (Figure 2a). This analysis illustrates
256 that, from any given cell on a river or ridge, the highest probabilities of finding an

257 adjacent upstream river or ridge cell occur in the three cells oriented toward the
 258 fan apex (Figure 2a).

259 The weighting factor for the upstream random walk is calculated by the cosine
 260 of the angle between the azimuth to each neighbouring cell and the fan apex (Fig.
 261 2c). Thus, the weighted probability P to connect a target aquifer cell with its
 262 neighbours is defined as:

$$P = A + B\cos(C\alpha) \quad (1)$$

263 where α is the angle between a straight line towards the apex and the azimuth
 264 to the neighbouring cell. The constant A is set to 0.05, representing the minimum
 265 probability observed from the elongated ridges (0.04 in Figure 2a). The constant
 266 B is 0.35 so the maximum probability is 0.4 ($A + B$), which is based on the high-
 267 est probabilities observed from the adjacent cells of the Sutlej and Yamuna river
 268 (0.413 in Figure 2a). The constant C is set to 1.4 to limit the span of the ran-
 269 dom walk to 130 degrees as observed on both the Sutlej and Yamuna fans. The
 270 weighted probability is calculated for all 8 neighbouring cells. Negative values
 271 are set to zero, and the probabilities for all directions that fall between alpha val-
 272 ues of -90 and 90 degrees are set to a small but arbitrary value of at least 0.025,
 273 so that the random walk has at least four upstream cells to choose. The four di-
 274 rections are needed as in some cases the three direct upstream grid cells for the
 275 coarser grids are identified as non-aquifer from the observational data, leaving
 276 no alternative pathway toward the apex. Because P depends on α and thus on
 277 location, we rescale the values so that they sum to 1 for each set of neighbours.
 278 Also, to force connectivity between aquifer-body positions on the fan and the fan
 279 apex, the weighted random walk uses progressively higher probability values to-

wards the apex and P is recalculated after each step. The random walk towards the apex is first calculated from well locations that are closest to the apex, and then for those that are progressively further away. We terminate each random walk when it reaches the apex or when it encounters another previously-identified aquifer cell. In the downstream direction, we apply a simplified weighting factor with equal probabilities of 0.3 to the three neighbouring cells away from the fan apex, and a small probability of 0.05 for the cells parallel to the mountain front (Figure 2d). This simplified scheme is used because there is not a fixed location (like the fan apex) where the random walk must end. The downstream random walk is applied in reverse order, so that well locations furthest away from the fan apex are analysed first. Each walk terminates when it encounters another previously-identified aquifer cell or when it reaches the model boundary (see boundary in Figure 1). Because the order of the random walk may affect the resultant probabilities, we also test a model in which the order was reversed, as well as a model that operates on well locations in a randomly sequence.

Our second assumption is that aquifer bodies, while continuous in the down-fan direction between the fan apex and points on the fan, are highly discontinuous in the across-fan direction. Thus, assuming that our model grid cells are sized appropriately, the presence of aquifer material in one cell should mean that there is non-aquifer material in adjacent cross-fan cells (i.e., those with alpha values of c. ± 90 degrees). This assumption is likely to be true if shifts in the active channel system across the fan occur by avulsion near the fan apex. If, instead, the channel migrates laterally during fan deposition, then aquifer material would be expected in adjacent cells with little vertical separation. The lack of clear correlations between aquifer material in adjacent boreholes in our study area, as documented by

305 Van Dijk et al. (2016), appears to argue for a dominance of avulsion over lateral
306 migration in this system. Thus, after connecting all aquifer cells to an upstream
307 aquifer cell and eventually to the fan apex, all cells adjacent to those continuous
308 aquifer corridors are filled with non-aquifer material (Figure 2e).

309 After these steps, there remain some unfilled cells within the model grid —
310 that is, cells for which we have neither direct observation nor geomorphic rules to
311 determine whether they should contain aquifer or non-aquifer material. Our final
312 constraint is that the bulk model aquifer fraction must match that of the actual fan
313 system, as estimated from the aquifer-thickness logs. Thus, on the fans we fill
314 the remaining cells with aquifer material at random until the bulk aquifer fraction
315 matches the observed value of 0.4. Randomly-filled cells will not necessarily be
316 adjacent or connect to the main channel corridors. Cells in the interfan area, which
317 is not supplied by either the Sutlej or Yamuna rivers, are also filled randomly
318 to match the observed bulk aquifer fraction of 0.3. Once the observed aquifer
319 fraction value of 0.4 has been reached, any final remaining cells that have not
320 been identified as aquifer cells are filled with non-aquifer material to complete the
321 depth slice.

322 3.2. *Model parameters and sensitivity*

323 The model is governed by several parameters: the number of realizations, the
324 grid cell size, the slice thickness, and the minimum aquifer thickness. Each model
325 realization produces a single solution of the distribution of aquifers in each depth
326 slice, which can be thought of as a map of aquifer locations that contains only
327 zeros (non-aquifer) and ones (aquifer). We perform Monte Carlo-type iterations
328 to produce probabilities in the range [0,1], defined for each cell as the fraction of
329 realizations that give rise to aquifer material in that cell. We vary the number of

330 realizations between 1 and 250 to test how that affects the cumulative probability
331 distribution.

332 Given our assumptions, the grid cell size should be limited to the typical lat-
333 eral dimensions of the potential aquifer bodies. Van Dijk et al. (2016) showed that
334 both the elongate palaeochannel ridges and the modern channel belts on the fan
335 surfaces vary between 2-10 km wide, whereas channel-body thickness-width scal-
336 ing relations are likely to be $\sim 1:1000$, suggesting a maximum width of about 6 km
337 for a median aquifer-body thickness of 6 m (Gibling, 2006). We perform simu-
338 lations with variable grid resolutions from 2 km to 8 km grid spacing, related to
339 the various channel width interpretations, to understand the resulting differences
340 and uncertainties in aquifer distribution. Most of the results shown here are based
341 on a cell size of 6 km, which relates to the median aquifer body thickness. While
342 it would certainly be possible to allow channel-belt widths to vary in space (e.g.,
343 Rongier et al., 2014), we make the simplifying assumption that they are fixed and
344 uniform. This is justified for two reasons: we lack any data on channel-width vari-
345 ations in space within the subsurface of these fans, making any spatial variations
346 arbitrary; and we do not know, a priori, whether the CGWB aquifer-thickness logs
347 have penetrated the aquifer bodies near their centres or near their margins, so that
348 definition of a true width in space would be very uncertain. An additional reason
349 for using a low-resolution grid is that much of the CGWB data on aquifer per-
350 formance (including estimated abstraction rate, potential evapotranspiration, and
351 recharge) are available on, at most, a block level. The mean block area in Punjab
352 and Haryana states is about 360 km^2 (10 model grid cells at a 6 km spacing), so
353 there is little rationale for a substantially higher model resolution. Conversely,
354 model outcomes and predictions can be fairly easily adapted to the block scale if

355 required.

356 Likewise, the slice thickness is chosen to scale with the median (or mean)
357 aquifer-body thicknesses observed in the Sutlej and Yamuna fan systems, which
358 are 6 m and 9 m across the study area, respectively (Van Dijk et al., 2016). Slice
359 thicknesses of 5 and 10 m give quantitatively similar simulation results for the
360 two-dimensional aquifer network, for simplicity we use 10 m depth slices for
361 most tests of model sensitivity and cross-validation. For analysis of the three-
362 dimensional representation of subsurface aquifers, in contrast, we use 5 m depth
363 slices as this will give a more accurate connectivity measure in the vertical direc-
364 tion.

365 The accuracy of the model is determined by the number and distribution of
366 observations that are used to populate the known aquifer and non-aquifer grid cells
367 in the first model step. Because aquifer-thickness logs are not evenly distributed
368 and the distance is sometimes smaller than the grid size, multiple logs may occur
369 in a single grid cell. For example, for a 6 km grid spacing, several log locations
370 fall within the same cell, so that, while there are 208 logs on the fan surface,
371 only 59 cells of the 884 cells of the Sutlej fan and 90 cells of the 695 cells in the
372 Yamuna fan are known from the observational data. Thus, we assign each cell
373 value based on the predominance of either aquifer or non-aquifer material in that
374 cell and depth slice. In most cases, we assign the cell as aquifer when at least one
375 of the logs is composed predominantly of aquifer material within that depth slice.
376 This approach is justified by the limited lateral extent of the aquifer bodies; logs
377 near the centre of a body would record its full thickness, but logs near its margins
378 would record only a portion of its total thickness and might be dominated by non-
379 aquifer material, even in the same cell and depth slice. To test the sensitivity of

380 our results to this approach, we also run an alternative algorithm that classifies a
381 cell as non-aquifer if at least one of the logs is composed predominantly of non-
382 aquifer material. We also test the extent to which the model results are influenced
383 by thin aquifer bodies — that is, units that may reflect terminal (crevasse) splays
384 or small plains-fed channels draining the fan surfaces rather than deposits of the
385 major rivers, and for which our model assumptions may therefore not be valid. To
386 do this, we run alternative model scenarios where we ignore aquifer bodies in the
387 input logs that are thinner than the median thickness of 6 m when populating the
388 model space.

389 3.3. Model analysis

390 3.3.1. Cross-validation

391 True validation of the model is impossible because the actual aquifer locations
392 are unknown. Therefore, we first assess the performance of the model by apply-
393 ing it to a test case of a two-dimensional image of a channel network. As the test
394 case image, we use the network of ridges on the surface of the Sutlej fan (Fig-
395 ure 1), inferred by Van Dijk et al. (2016) to represent a set of abandoned sand-rich
396 palaeochannels that radiate from the Sutlej fan apex. We interpolate these ridges
397 onto a grid with a spacing of 2 km (similar to the maximum observed 2.3 km
398 width of the ridges Van Dijk et al. (2016)) and classify ridge locations as aquifer
399 material, which fills about 25% of the grid. The remainder of the grid is classified
400 as non-aquifer material, completing the test case (Figure 3a). We then remove a
401 subset (80-95%) of the image at random, and use the remaining 5-20% as the start-
402 ing point for our model (Figure 3b). We compare the model results (Figure 3c)
403 to both the test case (Figure 3a) and to a null model (Figure 3d), created by sim-
404 ple random filling of the grid with aquifer material with the same bulk aquifer

405 fraction; both our model and the random filling model are run 100 times. This
406 gives a probability map for both our model (Figure 3e) and random filling (Fig-
407 ure 3f). Subsequently, the probability maps can be converted back to an aquifer
408 location map by applying a probability threshold μ , such that probabilities above
409 the threshold are classed as aquifer material and those below as non-aquifer. The
410 threshold is inversely proportional to the model-predicted bulk aquifer fraction
411 (f_μ); high thresholds will yield low aquifer fractions, and vice versa.

412 To quantitatively compare these probability maps, with values in the range of
413 [0,1], we calculate receiver operating characteristic (ROC) curves to assess the
414 model fit to the reserved subset of palaeochannel positions. The ROC curve is a
415 graphical plot that illustrates the performance of a binary classifier system (in this
416 case, aquifer and non-aquifer) as the probability threshold μ is varied. The curve is
417 created by plotting the true positive rate (TPR), defined as the number of cells that
418 are aquifer in both the predictive model and the data divided by number of actual
419 aquifer cells, against the false positive rate (FPR), defined as the number of cells
420 that are aquifer in the predictive model but non-aquifer in the data divided by the
421 number of non-aquifer cells. The TPR and FPR are calculated for various values
422 of μ . Increasing μ leads to fewer cells being classified as model aquifers, and
423 should lead to a decrease in both TPR and FPR. ROC curves are constructed for
424 both the model outputs and random filling of the grid. An effective model should
425 show a higher TPR at a given FPR than random filling, and the TPR should also
426 improve as a larger fraction of the available data is used to generate the model.

427 Comparison of the model results with the test case tests the ability of the model
428 to produce aquifer corridors comparable to the elongated ridges in terms of their
429 spatial distribution. Testing the ability of the model to generate a realistic distribu-

430 tion of potential aquifer bodies in the subsurface is more complicated, as we lack
431 full three-dimensional information on aquifer bodies across the study area. We
432 therefore assess the model performance by removing a random subset (10-50%)
433 of the CGWB aquifer-thickness logs to use as a test data set before running the
434 model. We then compare the model predictions at the test log positions against the
435 actual observations. To avoid any potential bias introduced by our choice of test
436 logs, we run 50 simulations with different subsets of test logs. The outcomes are
437 then compared to a random filling approach using the ROC curves. Furthermore,
438 we also construct separate ROC curves for the proximal (< 100 km from the fan
439 apex) and distal (> 100 km from the fan apex) parts of the fans, to investigate
440 whether the model performance is position-dependent.

441 3.3.2. *Subsurface stratigraphy and connectivity*

442 To compare the model outcomes for multiple realizations with the statistical
443 analysis of aquifer thickness data of Van Dijk et al. (2016), we need to create
444 a three-dimensional representation of the subsurface stratigraphy. Therefore, we
445 stack the individual depth slices and apply the probability threshold μ to convert
446 aquifer probability to the presence or absence of aquifer material. The value of
447 μ is chosen so that the model-predicted bulk aquifer fraction (f_{mu}) of the multiple
448 realizations is the same as the bulk aquifer fraction (f_{obs}) of the CGWB aquifer-
449 thickness data. Aquifer-body thicknesses are then calculated for all grid cell loca-
450 tions from the stacked depth slices and compared to the aquifer-body thicknesses
451 from the original logs. To examine the spatial distribution of potential aquifer
452 bodies, we also extract medial and distal cross sections oriented parallel to the Hi-
453 malayan mountain front (see Figure 1 for locations). The medial transect includes
454 logs that are located 50-110 km from the mountain front, while the distal transect

455 includes logs that are 160-250 km from the mountain front.

456 The three-dimensional stack from the multiple realizations also contains in-
 457 formation about the connectivity of the potential aquifer bodies within the subsur-
 458 face. Aquifer-body connectivity directly affects pumping or recovery, especially
 459 in regions with an intermediate proportion of aquifer bodies (Allen, 1978; Renard
 460 and Allard, 2013) such as our study region. Because the model builds potential
 461 aquifer bodies that are continuous down-fan and are surrounded by non-aquifer
 462 material, horizontal connectivity is to an extent hard-wired into the model outputs.
 463 The vertical connectivity is not pre-determined, however, nor is the connectivity
 464 between adjacent aquifer corridors. Here, we test model (multiple realizations)
 465 connectivity for various values of μ , compared to the results of random filling.
 466 We characterise these by the model-predicted bulk aquifer fraction (f_μ), which is
 467 inversely proportional to μ , as this makes it possible to directly compare the out-
 468 comes from our model with random filling. The range in μ for random filling is
 469 smaller and is generally lower compared to our model. We characterize connec-
 470 tivity by applying a commonly-used scalar index Γ that defines the probability of
 471 connection between two potential aquifer body cells (Larue and Hovadik, 2006;
 472 Hovadik and Larue, 2007), and is calculated as:

$$\Gamma = \frac{\sum_{i=0}^n (V_i^2)}{(\sum_{i=0}^n V_i)^2} \quad (2)$$

473 where V_i is the volume of an individual body and n is the total number of
 474 potential aquifer bodies. In the case of a single aquifer body, this probability is
 475 1, as the volume of the single aquifer is equal to the total aquifer-body volume.
 476 As the number of aquifers increases, or equivalently as the bulk aquifer fraction

477 increases, the connectivity index is initially low but then increases as clusters of
478 connected aquifer bodies are formed (Stauffer and Aharony, 1992; Christensen
479 and Moloney, 2005; Hovadik and Larue, 2007). High connectivity implies fewer
480 but larger clusters, with a high probability that any two cells are connected within
481 a cluster (Hovadik and Larue, 2007). For example, Γ for a system of 10 individual
482 aquifer bodies with a volume of 1 cell each will be 0.1, whereas a system with the
483 same aquifer fraction but comprising 1 body with a volume of 10 cells will give a
484 Γ of 1.

485 We allow connectivity between adjacent cells along faces, edges, and vertices
486 (26 possibilities), although other rules give qualitatively similar results. We cal-
487 culate the connectivity index for various values of μ (or equivalently for different
488 f_μ), for both the model output and the case of random filling. We plot poten-
489 tial aquifer body connectivity within the subsurface stratigraphy for two down-fan
490 sections, normal to the mountain front, and three across-fan sections parallel to
491 the mountain front, in order to compare the two models (Figure 4a).

492 4. Results

493 4.1. Model output

494 A single realization of the model produces a map that contains only zeros and
495 ones — that is, aquifer and non-aquifer material (Figure 4a). Running multiple
496 realizations yields a probability of finding aquifer material (with values in the
497 range $[0,1]$) at every location within the region of interest (Figure 4b). Increasing
498 the number of realizations leads to a smoother cumulative probability distribution
499 (Figure 4c). There is little difference, however, between the cumulative probab-
500 ility distributions for 100 and 250 realizations (Figure 4d). The model algorithm

501 is coded in MATLAB, and a typical 100-realization run for a 6 x 6 km grid on a
502 standard desktop computer takes on the order of 10 seconds per depth slice. The
503 aquifer probability values are affected by the processing order of the random walk.
504 In the cases of a reversed processing order (i.e., starting with aquifer cells farthest
505 from the apex) or a randomly-chosen sequence, aquifer pathways are more likely
506 to be parallel toward the fan apex rather than intersecting, because the space near
507 the apex is not filled as quickly, so that aquifer probability values are generally
508 slightly higher.

509 4.2. Sensitivity to channel width

510 Most of the model runs were carried for a channel width interpretation of 6
511 km represented by 6 x 6 km grid cells. A decrease in the channel width, i.e., the
512 grid size to 2 x 2 km, equivalent to the maximum width of the elongated fan sur-
513 face ridges (Table 1), shows that the probability of finding aquifer material at any
514 given cell generally decreases (Figure 5a), and provides some additional infor-
515 mation on the likelihood of finding potential aquifer bodies within the large-scale
516 corridors identified on the lower-resolution grid (Figure 4c). Runs for smaller
517 channel widths, i.e., higher grid resolutions, yield larger uncertainties for points
518 that are well away from the known log locations. Reducing the channel width and
519 increasing the number of grid cells also means that a larger area must be randomly
520 filled to obtain a bulk aquifer fraction of 0.4 on the fans (Figure 5b). This effect
521 is not straightforward, though, because of the geometry of the potential aquifer
522 bodies in the model. Although the number of cells is increased by a factor of 9 for
523 a 2 x 2 km grid compared to the base configuration, the fraction of empty cells is
524 only increased by 4.5 times (Figure 5b). This is because, with a coarser grid, the
525 spacing between two adjacent aquifer corridors may be less than 2 grid cells, so

526 that fewer adjacent cells are filled with non-aquifer material compared to the finer
527 grid.

528 4.3. Sensitivity to the input data

529 Reconstruction of aquifer corridors depends on the precedence given to the in-
530 put data. When a cell is classified as aquifer material, then a corridor is created and
531 propagated upstream and downstream, but when a cell is classified as dominantly
532 non-aquifer material, then there are no rules that are used to set the surrounding
533 cells. This affects the number of empty cells after applying our model rules and
534 eventually the number of cells that are randomly filled. Thus, the number of empty
535 cells varies with depth slices, showing fewer empty cells for the top 100 m (Fig-
536 ure 5c). Further, there are more empty cells (that must then be randomly filled)
537 when non-aquifer material is given precedence for cells with multiple logs (Fig-
538 ure 6a). This change causes a decline in the high aquifer probabilities associated
539 with connected aquifer corridors on both fans (see the blue colours in Figure 6b).

540 Assignment of a cell as aquifer or non-aquifer material is based on aquifer
541 bodies that vary in thickness from 1 m up to 80 m. While it is unlikely that
542 the thinnest aquifer bodies were deposited by major river systems that were con-
543 nected with the fan apex (as required by our model assumptions), simulations that
544 ignore aquifer bodies of less than 6 m thickness show no significant changes in the
545 number of empty cells left in the model or in the overall pattern of aquifer proba-
546 bilities (Figure 5d). This means that the same area is filled by our algorithm, i.e.,
547 the model outcome is not greatly affected by the thinnest aquifer bodies, probably
548 because they make up a small fraction of each 10 m depth slice.

549 *4.4. Model performance cross-validation*

550 The ROC curves allow us to examine three separate aspects of the model: the
551 effect of the threshold μ used to convert aquifer probability into aquifer pres-
552 ence or absence, the effect of the removal of an increasing proportion of the input
553 logs to validate the model results, and the differences in performance between the
554 model and random filling. In the case of random filling, increasing the threshold
555 (that is, increasing the probability value needed to assign aquifer material to a cell
556 in the final map) causes a proportionate decrease in both TPR and FPR, so that
557 the ROC curve is approximately a straight line (Figure 7a). The model, however,
558 performs better for increasing threshold values, as shown by the increasing ratio
559 of TPR to FPR (Figure 7a-d). Removal of an increasing fraction of the input data
560 has little effect on the ROC curves in the case of random filling, as it causes lit-
561 tle relative change in the number of cells that are randomly filled (Figure 7a-c).
562 For the model, however, removal of an increasing fraction of input data causes
563 the ROC curves to shift noticeably towards the random filling curves, because a
564 greater number of cells must be filled randomly.

565 Overall, the model shows a higher TPR-FPR ratio than the case of random fill-
566 ing for high probability thresholds, particularly when used to reproduce the elon-
567 gate palaeochannel ridges on the Sutlej fan (Figure 7a). Random filling yields
568 a higher TPR than the model, however, for low threshold values, especially for
569 the CGWB input logs (Figure 7b-c). A total of 50 simulations including differ-
570 ent randomly-chosen subsets of the data shows that the model generally performs
571 very well compared to random filling, with a TPR of 0.5 over a FPR of 0.2. How-
572 ever, selecting a different subset of the data could lead to a poor solution as well
573 (Figure 7c), but overall the model performs better than random filling. Compar-

574 ison of the ROC curves from different parts of the fan shows that the TPR-FPR
575 ratio is higher, especially for conservative threshold values, i.e., when FPR is low,
576 for the proximal part of the fan (Figure 7d). This means that model performance,
577 relative to the case of random filling, is somewhat reduced for distal locations.

578 4.5. Sand-body connectivity

579 A single realization of the model forms elongate ‘ribbons’ that are, by design,
580 well-connected in the down-fan direction, but less so in the across-fan direction.
581 Unfortunately, we cannot compare the connectivity of our model after multiple
582 realizations results with independent connectivity estimates. Instead, we examine
583 the sensitivity of the connectivity index to the threshold μ (or f_μ), and determine
584 the μ value at which the model output behaves as an isotropic aquifer. We compare
585 the model results (Figure 8) to results from the case of random filling along several
586 different cross sections.

587 The potential aquifer bodies created by the model are generally more con-
588 nected than those generated by random filling, except at low values of μ , equiva-
589 lent to high f_μ (Figure 8a). In both cases, the index increases rapidly for moderate
590 f_μ , as isolated potential aquifer bodies become clustered. This transition occurs at
591 f_μ of 0.1-0.3 for the model as well as for random filling (Figure 8a). This analysis
592 shows that for both approaches, potential aquifer bodies are highly isotropically
593 connected for f_μ of 0.4 or greater.

594 The model predicts that aquifer body connectivity in the down-fan direction
595 should be similar to or greater than connectivity in the across-fan direction, as we
596 would expect to see in a fan system, especially for f_μ values of 0.4 or greater (Fig-
597 ure 8b). At lower f_μ , the model predicts greater across-fan connectivity, especially
598 in proximal and medial sections compared in distal sections (Figures 8b). Thus,

599 we should expect a greater degree of across-fan connectivity near the fan apices,
600 because potential aquifer bodies are constrained to converge at the apex and com-
601 bine to a big aquifer with high connectivity. The proximal section, however, is less
602 connected as expected because of low values in the interfan area between both fan
603 systems. In contrast, random filling of aquifer material gives rise, unsurprisingly,
604 to connectivity that is essentially isotropic in both the down-fan and across-fan
605 directions (Figure 8c), and is unable to reproduce the connectivity patterns that
606 we might expect in fan settings.

607 **5. Discussion**

608 The model simulations yield probability maps of finding aquifer locations
609 within a series of depth slices. Stacking the depth slices together gives informa-
610 tion on the likely spatial distribution of high aquifer probabilities in the subsurface.
611 We first relate the modelled distribution to our expectation of fan stratigraphy in
612 general, and our understanding of the Sutlej-Yamuna fan system (Van Dijk et al.,
613 2016) in particular. We also consider the possible uses and limitations of the
614 model, and some ideas for how it could be improved.

615 *5.1. Relation between model results and subsurface stratigraphy of the Sutlej-* 616 *Yamuna fans*

617 Recall that the model contains no specific rules about sediment transport, de-
618 positional processes, or fan construction; instead, it uses some knowledge of the
619 lateral and vertical dimensions of individual aquifer bodies along with their spa-
620 tial disposition. Because the model rules are focused on individual aquifer units,
621 it is not necessarily clear that the model-derived stratigraphy — which consists

622 of a stack of individual aquifer units — will provide a physically-reasonable rep-
623 resentation of regional stratigraphy. Thus, it is instructive to compare the model
624 stratigraphy with both a theoretical expectation of fan stratigraphy and our obser-
625 vations of subsurface aquifer-body distributions in the study area (Van Dijk et al.,
626 2016). To do this, the model outputs for each 5 m depth slice are stacked to repre-
627 sent the probabilistic aquifer-body distribution for the top 200 m of the subsurface.
628 We then apply a threshold μ to transform the probability values to modelled po-
629 tential aquifer bodies in a three-dimensional volume. The size and spatial pattern
630 of those bodies is dependent on the applied μ , such that potential aquifer bodies
631 are both thicker and more numerous for a lower μ (Table 3). For a μ of 0.45,
632 meaning that a modelled aquifer cell is simulated as aquifer material in at least
633 45% of the iterations, the quantiles of the aquifer thickness distribution (25th, 50th
634 and 75th percentiles) as well as the f_μ are closest to their observed values based
635 on the aquifer-thickness logs (Table 2, Van Dijk et al., 2016). Interestingly, this μ
636 also corresponds to the highest ratio of TPR to FPR within the ROC curve (Fig-
637 ure 7b). We therefore apply this μ in our further analysis of the modelled potential
638 aquifer bodies below.

639 Conceptual fan models often indicate a general decrease in the lateral dimen-
640 sions of the sand bodies in downstream direction (e.g., Friend, 1978; Nichols and
641 Fisher, 2007; Cain and Mountney, 2009; Weissmann et al., 2013; Owen et al.,
642 2015). Near the fan apex, we would expect little preservation of associated fine-
643 grained overbank deposits, and channel deposits are likely to be stacked or amal-
644 gamated (Friend, 1983). Away from the apex, conceptual models predict that the
645 proportion of overbank deposits should increase and the dimensions of channel
646 deposits should decrease. In agreement with this expectation, the interpolated

647 aquifer probabilities are generally higher along the medial transect (Figure 9a)
648 compared to the distal transect (Figure 9b). Both transects, but especially the me-
649 dial one, contain high probabilities of aquifer material along corridors that are
650 collectively more than 6 km wide, i.e., more than the grid resolution associated
651 with 6 km wide channel belts. These corridors could be due to (i) amalgamation
652 of multiple individual potential aquifer bodies, (ii) interpolation onto the tran-
653 sect, oblique to the grid direction, or (iii) interpolation of multiple realizations
654 creating high probabilities around known well locations. An alternative approach
655 that would reduce interpolation effects would be to use an object-based model,
656 combining the random walk to define the channel pathways with an assumption
657 about channel belt width and thickness at each point. This approach has been suc-
658 cessfully applied to construct 3D karst conduits in the subsurface (Rongier et al.,
659 2014).

660 Conceptual fan models also suggest that a downstream decrease in aquifer-
661 body thickness should be expected because of channel termination or bifurca-
662 tions (e.g., Friend, 1978; Nichols and Fisher, 2007). Owen et al. (2015) showed,
663 however, that for Jurassic fan systems of the Morrison Formation in the western
664 U.S.A., the channel size did not significantly change down fan but that the per-
665 centage of fines increased. This is also observed in the Yamuna fan but less in the
666 Sutlej fan (Van Dijk et al., 2016); the aquifer thickness distribution remains simi-
667 lar with distance from the fan apices, but the fraction of aquifer bodies decreases.
668 Van Dijk et al. (2016) interpreted this pattern as a simple volumetric consequence
669 of the conical fan shape combined with a near-uniform size of the aquifer bodies
670 across the study area, perhaps due to stacking of channel belts or filling of incised
671 valleys. A similar analysis of the aquifer-body thickness distribution derived from

672 the model results shows no decrease in aquifer-body thickness down fan, similar
673 to the observations from the Yamuna fan (Table 4). It must be remembered that
674 our model aquifer thicknesses are multiples of 5 m, so that quantitative compar-
675 isons with real aquifer-thickness distributions must be made with caution.

676 Fan models also encompass the connectivity of sand bodies within the sub-
677 surface stratigraphy, which enables fast flow and transport from one location to
678 another (Larue and Hovadik, 2006; Renard and Allard, 2013). Horizontal con-
679 nectivity is partially set by the model rules, because we assume that individual
680 bodies are continuous down-fan, are no more than one grid cell in width, and
681 are bounded by finer-grained non-aquifer material, but in practice the horizontal
682 connectivity depends also on the density of aquifer cells in the input data. The
683 extent of vertical connectivity between the bodies should increase as the proba-
684 bility threshold μ (which controls the model-predicted bulk aquifer fraction, f_{μ})
685 is increased. Our analysis shows that sand bodies for both approaches are fairly
686 well connected throughout the basin (Figure 8b), but the connectivity differs in
687 cross-fan and down-fan direction for our model compared to random filling (Fig-
688 ure 8c-d). Our model has reasonably high connectivity in the cross-fan direction,
689 despite the fact that the model is actually hard-wired against cross-fan connection.
690 There is no difference in connectivity between our model and random filling for
691 aquifer systems with a bulk aquifer fraction (f_{obs}) of more than ~ 0.5 (Figure 8c-
692 d). This suggests that the model has no additional skill for predicting connectivity
693 within a highly sand-dominated system — for example, the Kosi fan in northern
694 India, with a bulk aquifer fraction of 0.89 (Sinha et al., 2014).

695 5.2. *Potential use and future improvements of the model*

696 The model provides a tool to estimate the probability of finding aquifer mate-
697 rial within a near-surface volume, based on information at known well locations
698 and some simplified geological knowledge about the origin, depositional pattern,
699 and likely dimensions of aquifer bodies. The model could be used in a generic
700 sense to understand the potential variations in subsurface aquifer distribution and
701 connectivity in cases of variable bulk aquifer fractions. Because we have popu-
702 lated the model with actual data on aquifer-body positions taken from the CGWB
703 aquifer-thickness logs, however, it is also useful as a predictive tool to generate
704 probabilities of encountering aquifer bodies at any point, and at any given depth,
705 across the study region. The model algorithm strikes a balance between purely
706 empirical (and computationally simple) approaches on the one hand, and process-
707 based but more computationally-intensive approaches on the other. Because of
708 its simplicity, it can easily be updated to incorporate new subsurface information
709 on aquifer-body positions (e.g., from new boreholes), as that simply increases the
710 number of ‘known’ cells at the start of the model run. There is no need to redefine
711 the geometry of potential aquifer bodies or channel pathways in the subsurface, as
712 that is done automatically, and because model run times are short the model can
713 be quickly re-run to reflect evolving knowledge.

714 Encouragingly, the model performs best when compared to random filling at
715 low false-positive rates, corresponding to a high value of the probability thresh-
716 old μ that is used to convert aquifer probability into the presence or absence of
717 model aquifers (Figure 7b-c). A conservative strategy for identifying target ar-
718 eas for new wells would seek to minimise false-positives (i.e., locations where
719 the model predicts aquifer material at a given depth, but none is found), and un-

720 der those constraints the model substantially outperforms random filling. The
721 model could thus be employed as a guide to prioritise the siting of new wells. It
722 could be combined with, for example, magnitude-frequency analysis of aquifer-
723 thickness data (Van Dijk et al., 2016) to also provide information on the prob-
724 ability of encountering an aquifer body of a given thickness at those new well
725 locations. The more specific effects of the 3D subsurface stratigraphy generated
726 by the model on groundwater flow and transport, and the quantitative differences
727 between model stratigraphy and that generated by random filling, would need to
728 be tested with regional-scale hydrogeological modelling (e.g., Ronayne and Gore-
729 lick, 2006; Burns et al., 2010). It would also be useful to perform groundwater
730 flow and transport simulations on the various individual realizations instead of the
731 probability maps, which could for example yield information on uncertainty in
732 contaminant propagation prediction. This application might need refinement of
733 the grid to avoid numerical artefacts. Refinement could be done either for individ-
734 ual realizations or by adapting our model algorithm. For example, we could apply
735 the algorithm on a finer grid, then fill adjacent cells perpendicular to the random
736 walk to obtain an aquifer of 6 km wide before continuing our algorithm.

737 There are a number of areas of the model that could be improved or refined.
738 The surface test case of the elongated ridges shows that there is good performance
739 when 10% of the fan area is covered with data. However, the performance for
740 the subsurface is less accurate. The two different data sets are recording differ-
741 ent things; the ridges are fluvial, open fan channels, while the reserved logs are
742 recording aquifer bodies. We have inferred that the surface ridges are a good ana-
743 logue for subsurface channel bodies because of their scale and pattern (radiating
744 from the fan apex). The subsurface, however, contains some incised-valley fills,

745 which may not be represented by the surface ridges, and which may have different
746 preservation potential in the subsurface (Weissmann et al., 1999).

747 While the regional coverage of our aquifer-thickness data is extensive, the logs
748 are still relatively sparse, and the model is forced to fill many gaps even on our
749 low-resolution 6 x 6 km grid. This grid spacing is based on likely aquifer-body
750 widths as inferred from surface observations in the study area (Van Dijk et al.,
751 2016). There is substantial uncertainty on those widths, stemming from both the
752 range of channel deposit widths visible at the surface and the viability of surface
753 features as an appropriate analogue for subsurface aquifer bodies. For example,
754 the elongated surface ridges that are used as an analogue for subsurface channel
755 deposits are only 500-2500 m wide (Van Dijk et al., 2016), meaning that a 2-3 km
756 grid might allow for more precise delineation of potential aquifer bodies. This
757 would lead, however, to a dramatic increase in the number of empty cells that
758 the model must fill (Figure 5b), and clearly we lack the subsurface data to test
759 the advantages of a more precise model result in any quantitative way. The ROC
760 curve shows that the distal part of the fan is already less accurately predicted with
761 the current data availability (Figure 7d). Poor model performance could also be
762 caused by the fact that we neglect the local surface topography and assume that
763 the modern basin surface slope is the same as the slope throughout fan deposi-
764 tion. An improvement would be to obtain actual local surface topography and
765 use a different reference elevation for connecting the various logs. Finally, we
766 caution that the model algorithm, while flexible and potentially portable to other
767 fan settings, has been designed with the Sutlej-Yamuna fan system in mind. At
768 the very least, application to other fans would require some preliminary analysis
769 of available aquifer-thickness data and observations of channel-belt dimensions

770 and deposit widths, in order to set both the depth slice thickness and model grid
771 size to appropriate values. The model sensitivity to the bulk aquifer fraction (Fig-
772 ures 7, 8) also shows that, for systems with a high aquifer fraction, the model
773 provides little additional information or skill over simple random filling, because
774 the likelihood of finding aquifer material is high everywhere. Thus, application to
775 this type of fan system, such as the Kosi fan, does not appear warranted.

776 **6. Conclusions**

777 We have shown that the subsurface distribution of aquifer corridors across the
778 Sutlej and Yamuna fans in northwestern India can be reconstructed by a reduced-
779 complexity probabilistic model that incorporates some degree of geological knowl-
780 edge of the depositional system. The model connects known locations of aquifer
781 material with the fan apex by a weighted random walk, and uses the assumed
782 lateral dimensions of the major aquifer bodies to identify likely locations of non-
783 aquifer material to either side of the aquifer corridors. The model is sensitive to
784 the type and distribution of input information, and the addition of new subsur-
785 face data can cause a substantial decrease in the number of empty cells that must
786 be filled by the model. Cross-validation of the model against a subset of input
787 CGWB aquifer-thickness logs indicates that the model provides an increase in the
788 true-positive rate compared to simple random filling of the basin, especially for
789 moderate to high values of the threshold used to convert aquifer probability into
790 model aquifer position.

791 The model produces a simplified representation of the subsurface stratigraphy
792 across the study area that matches key aspects of the spatial distribution of aquifer
793 thicknesses (Van Dijk et al., 2016). The results show that aquifer-body probability

794 is highest near the fan apices, as multiple channel systems must be routed through
795 a relatively small area, compared with lower probabilities in distal regions. This
796 high probability in proximal regions is also reflected in the high connectivity be-
797 tween potential aquifer bodies in the across-fan direction, normal to the transport
798 direction, despite the fact that the model rules militate against lateral connectivity.
799 In general, predicted aquifer connectivity is higher and more anisotropic for the
800 model-derived stratigraphy than for the case of random filling, especially at low
801 to moderate bulk aquifer fractions like those found in the study area.

802 The model could be used to explore variations in aquifer-body distribution
803 at different aquifer fractions, or to predict the likelihood of finding aquifer ma-
804 terial at a given location and depth across the study region. Importantly, model
805 performance increases as more data are incorporated, meaning that information
806 from new boreholes could be used to iteratively increase the model accuracy as
807 new parts of the system are explored. The model could also be applied to other
808 fan-hosted aquifer systems, although some caution is needed in ensuring that the
809 geological rule set remains valid and that appropriate model dimensions are cho-
810 sen.

811 **7. ACKNOWLEDGEMENTS**

812 This project is supported by the UK Natural Environment Research Council
813 and the Indian Ministry of Earth Sciences under the Changing Water Cycle-South
814 Asia program (grant NE/I022434/1). We gratefully acknowledge Sanjeev Gupta
815 for many helpful and insightful discussions. We thank Tejdeep Singh of the Cen-
816 tral Groundwater Board, Chandigarh, for providing the aquifer thickness data for
817 Punjab and Haryana. Constructive and positive reviews by Meredith Reitz and

818 two anonymous reviewers, Associate Editor Niklas Linde, and Editor Peter Ki-
819 tanidis helped to clarify and strengthen the manuscript. To obtain the data and
820 Matlab code used in this paper, please contact the authors.

References

- Allen, J.R.L., 1978. Studies in fluvial sedimentation: an exploratory quantitative model for the architecture of avulsion-controlled alluvial studies. *Sedimentary Geology* 21, 129–147. doi:10.1016/0037-0738(78)90002-7.
- Allen, J.R.L., 1979. Studies in fluvial sedimentation: an elementary geometric model for the connectedness of avulsion-related channel sand bodies. *Sedimentary Geology* 24, 253–267. doi:10.1016/0037-0738(79)90072-1.
- Anderson, M.P., 1989. Hydrogeologic facies models to delineate large-scale spatial trends in glacial and glaciofluvial sediments. *Geological Society of America Bulletin* 101, 501–511.
- Bridge, J.S., Leeder, M.R., 1979. A simulation model of alluvial stratigraphy. *Sedimentology* 26, 617–644. doi:10.1111/j.1365-3091.1979.tb00935.x.
- Bridge, J.S., Mackey, S.D., 1993. A revised alluvial stratigraphy model, in: Marzo, M., Puigdefabregas, C. (Eds.), *Alluvial sedimentation*, International Association of Sedimentologists Special Publication. pp. 319–336.
- Burns, E.R., Bentley, L.R., Hayashi, M., Grasby, S.E., Hamblin, A.P., Smith, D.G., Wozniak, P.R.J., 2010. Hydrogeological implications of paleo-fluvial architecture for the Paskapoo Formation, SW Alberta, Canada: a stochastic analysis. *Hydrogeology Journal* 18, 1375–1390. doi:10.1007/s10040-010-0608-y.

- Caers, J., 2001. Geostatistical reservoir modelling using statistical pattern recognition. *Journal of Petroleum Science and Engineering* 29, 177–188.
- Cain, S.A., Mountney, N.P., 2009. Spatial and temporal evolution of a terminal fluvial fan system: the Permian Organ Rock Formation, South-east Utah, USA. *Sedimentology* 56, 1774–1800. doi:10.1111/j.1365-3091.2009.01057.x.
- Chen, J., Famiglietti, J.S., Scanlon, B.R., Rodell, M., 2016. Groundwater storage changes: present status from GRACE observations. *Surveys in Geophysics*, 1–21doi:10.1007/s10712-015-9332-4.
- Chen, J., Li, J., Zhang, Z., Ni, S., 2014. Long-term groundwater variations in Northwest India from satellite gravity measurements. *Global and Planetary Change* 116, 130–138. doi:10.1016/j.gloplacha.2014.02.007.
- Christensen, K., Moloney, N.R., 2005. Complex and criticality, in: *Advanced Physics Texts Volume 1*, Imperial College Press, London. pp. 15–29.
- Comunian, A., Renard, P., Straubhaar, J., 2012. 3D multiple-point statistics simulation using 2D training images. *Computer and Geosciences* 40, 49–65. doi:10.1016/j.cageo.2011.07.009.
- Fogg, G.E., 1986. Groundwater flow and sand body interconnectedness in a thick multiple-aquifer system. *Water Resources Research* 22, 679–694.
- Friend, P.F., 1978. Distinct features of some ancient river systems, in: Miall, A.D. (Ed.), *Fluvial Sedimentology*, *Memoirs of the Canadian Society of Petroleum Geologist*. pp. 531–542.

- Friend, P.F., 1983. Towards the field classification of alluvial architecture or sequence, in: Collinson, J.D., Lewin, J. (Eds.), *Modern and Ancient Fluvial Systems*, IAS Special Publication. pp. 345–354. doi:10.1002/9781444303773.ch28.
- Galloway, W.E., 1981. Depositional architecture of Cenozoic Gulf coastal plain fluvial systems. *SEPM Special Publication* 31, 127–155.
- Gibling, M.R., 2006. Width and thickness of fluvial channel bodies and valley fills in the geological record: a literature compilation and classification. *Journal of Sedimentary Research* 76, 731–770. doi:10.2110/jsr.2006.060.
- Guardiano, F., Srivastava, R.M., 1993. Multivariate geostatistics: Beyond bivariate moments, in: Soares, A. (Ed.), *Proceedings of the 4th Annual International Geostatistical Congress – Geostatistics Troia '92*, Kluwer Academic Publishers, Norwell, Massachusetts, USA. pp. 133–144.
- Gupta, S., 1997. Himalayan drainage patterns and the origin of fluvial megafans in the Ganges foreland basin. *Geology* 25, 11–14.
- Hovadik, J.M., Larue, D.K., 2007. Static characterization of reservoirs: refining the concepts of connectivity and continuity. *Petroleum Geoscience* 13, 195–211.
- Isaak, E.H., Srivastava, R.M., 1990. *An introduction to applied geostatistics*. Oxford University Press, New York, USA.
- Jerolmack, D.J., Paola, C., 2007. Complexity in a cellular model of river avulsion. *Geomorphology* 91, 259–270. doi:10.1016/j.geomorph.2007.04.022.

- Jordan, D.W., Pryor, W.A., 1992. Hierarchical levels of heterogeneity in a Mississippi River meander belt and application to reservoir systems. *AAPG Bulletin* 76, 1601–1624.
- Journel, A., 1988. *Fundamentals of geostatistics in five lessons*. American Geophysical Union, Washington, D.C. USA. doi:10.1029/SC008.
- Karssenberg, D., Törnqvist, T.E., Bridge, J.S., 2001. Conditioning a process-based of sedimentary architecture to well data. *Journal of Sedimentary Research* 71, 868–879.
- Koltermann, C.E., Gorelick, S.M., 1996. Heterogeneity in sedimentary deposits: A review of structure-imitating, process-imitating, and descriptive approaches. *Water Resources Research* 32, 2617–2658.
- Van de Lageweg, W.I., Schuurman, F., Shimizu, Y., Cohen, K.M., Van Dijk, W.M., Kleinhans, M.G., 2016a. Preservation of meandering river channels in uniformly aggrading channel belts. *Sedimentology* 63, 586–608. doi:10.1111/sed.12229.
- Van de Lageweg, W.I., Van Dijk, W.M., Box, D., Kleinhans, M.G., 2016b. Archimetrics: a quantitative tool to predict three-dimensional meander belt sand-body heterogeneity. *The Depositional Record* 2, 22–46. doi:10.1002/dep2.12.
- Larue, D.K., Hovadik, J., 2006. Connectivity of channelized reservoirs: a modelling approach. *Petroleum Geoscience* 12, 291–308. doi:10.1144/1354-079306-699.
- Leeder, M.R., 1978. A quantitative stratigraphic model for alluvium, with spatial reference to channel deposit density and interconnectedness, in: Miall, A.D.

- (Ed.), *Fluvial Sedimentology*, Canadian Society of Petroleum Geologists Memoir. pp. 587–596.
- Liang, M., Geleynse, N., Edmonds, D.A., Passalacqua, P., 2015a. A reduced-complexity model for river delta formation – part 2: Assessment of the flow routing scheme. *Earth Surface Dynamics* 3, 87–104. doi:10.5194/esurf-3-87-2015.
- Liang, M., Voller, V.R., Paola, C., 2015b. A reduced-complexity model for river delta formation – part 1: Modeling deltas with channel dynamics. *Earth Surface Dynamics* 3, 67–86. doi:10.5194/esurf-3-67-2015.
- Mackey, S., Bridge, J., 1995. Three-dimensional model of alluvial stratigraphy: theory and application. *Journal of Sedimentary Research* 65B, 7–31.
- Malik, J.N., Mohanty, C., 2007. Active tectonic influence on the evolution of drainage and landscape: Geomorphic signatures from frontal and hinterland areas along the Northwest Himalaya, India. *Journal of Asian Earth Sciences* 29, 604–618. doi:10.1016/j.jseaes.2006.03.010.
- Mariethoz, G., Lefebvre, S., 2014. Bridges between multiple-point geostatistics and texture synthesis: Review and guidelines for future research. *Computers & Geosciences* 66, 66–80. doi:10.1016/j.cageo.2014.01.001.
- de Marsily, G., Delay, F., Gonçalves, J., Renard, P., Teles, V., Violette, S., 2005. Dealing with spatial heterogeneity. *Hydrogeology Journal* 13, 161–183. doi:10.1007/s10040-004-0432-3.
- Miall, A.D., 1985. Architectural-Element Analysis: A New Method of Facies Analysis Applied to Fluvial Deposits. *Earth-Science Reviews* 22, 261–308.

- Miall, A.D., 1988. Reservoir heterogeneities in fluvial sandstones: Lessons from outcrop studies. *AAPG Bulletin* 72, 682–697.
- Nemec, W., Steel, R.J., 1988. What is a fan delta and how do we recognize it?, in: Nemec, W., Steel, R.J. (Eds.), *Fan Deltas: Sedimentology and Tectonic Settings*, pp. 3–13.
- Nicholas, A.P., Sambrook Smith, G.H., Amsler, M., Ashworth, P.J., Best, J.L., Hardy, R.J., Lane, S.N., Orfeo, O., Parsons, D.R., Reesink, A.J.H., Sandbach, S.D., Simpson, C.J., Szupiany, R.N., 2016. The role of discharge variability in determining alluvial stratigraphy. *Geology* 44, 3–6. doi:10.1130/G37215.1.
- Nichols, G.J., Fisher, J.A., 2007. Processes, facies and architecture of fluvial distributary system deposits. *Sedimentary Geology* 195, 75–90. doi:10.1016/j.sedgeo.2006.07.004.
- Owen, A., Nichols, G.J., Hartley, A.J., Weissmann, G.S., Scuderi, L.A., 2015. Quantification of a distributive fluvial system: the Salt Wash DFS of the Morrison Formation, SW USA. *Journal of Sedimentary Research* 85, 544–561. doi:10.2110/jsr.2015.35.
- Price, W., 1974. Simulation of alluvial fan deposition by a random walk model. *Water Resources Research* 10, 263–274.
- Pyrcz, M.J., Catuneanu, O., Deutsch, C.V., 2005. Stochastic surface-based modeling of turbidite lobes. *AAPG Bulletin* 89, 177–191.
- Renard, P., Allard, D., 2013. Connectivity metric for subsurface flow and transport. *Advances in Water Resources* 51, 168–196. doi:10.1016/j.advwatres.2011.12.001.

- Rezaee, H., Mariethoz, G., Koneshloo, M., Asghari, O., 2013. Multiple-point geostatistical simulation using the bunch-pasting direct sampling method. *Computer & Geosciences* 54, 293–308. doi:10.1016/j.cageo.2013.01.020.
- Rodell, M., Velicogna, I., Famiglietti, J.S., 2009. Satellite-based estimates of groundwater depletion in India. *Nature* 460, 999–1002. doi:10.1038/nature08238.
- Ronayne, M.J., Gorelick, S.M., 2006. Effective permeability of porous media containing branching channel networks. *Physical Review* 73, 026305. doi:10.1103/PhysRevE.73.026305.
- Rongier, G., Collon-Drouaillet, P., Filipponi, M., 2014. Simulation of 3D karst conduits with an object-distance based method integrating geological knowledge. *Geomorphology* 217, 152–164. doi:10.1016/j.geomorph.2014.04.024.
- Sheets, B.A., Hickson, T.A., Paola, C., 2002. Assembling the stratigraphic record: depositional patterns and time-scales in an experimental alluvial basin. *Basin Research* 14, 287–301. doi:10.1046/j.1365-2117.2002.00185.x.
- Singh, A., Paul, D., Sinha, R., Thomsen, K.J., Gupta, S., 2016. Geochemistry of buried river sediments from Ghaggar Plains, NW India: Multi - proxy records of variations in provenance, paleoclimate, and paleovegetation patterns in the late quaternary. *Palaeogeography, Palaeoclimatology, Palaeoecology* 449, 85–100. doi:10.1016/j.palaeo.2016.02.012.
- Sinha, R., Ahmad, J., Gaurav, K., Morin, G., 2014. Shallow subsurface stratigraphy and alluvial architecture of the Kosi and Gandak megafans in

- the Himalayan foreland basin, India. *Sedimentary Geology* 301, 133–149. doi:10.1016/j.sedgeo.2013.06.008.
- Sinha, R., Yadav, G.S., Gupta, S., Singh, A., Lahiri, S.K., 2013. Geoelectric resistivity evidence for subsurface palaeochannel systems adjacent to Harappan sites in northwest India. *Quaternary International* 308-309, 66–75. doi:10.1016/j.quaint.2012.08.002.
- Stauffer, D., Aharony, A., 1992. *Introduction to Percolation Theory*. 2nd edn ed., Taylor & Francis, London.
- Stouthamer, E., 2005. Reoccupation of channel belts and its influence on alluvial architecture in the Holocene Rhine-Meuse delta, The Netherlands, in: *River Deltas – Concepts, Models, and Examples*, Special Publication, SEPM Special Publications. pp. 319-339.
- Straub, K.M., Paola, C., Mohrig, D., Wolinsky, M.A., George, T., 2009. Compensational stacking of channelized sedimentary deposits. *Journal of Sedimentary Research* 79, 673–688. doi:10.2110/jsr.2009.070.
- Strebelle, S., 2002. Conditional simulation of complex geological structures using multiple-point statistics. *Mathematical Geology* 31, 1–21. doi:10.1023/A:1014009426274.
- Sylvester, Z., Pirmez, C., Cantelli, A., 2011. A model of submarine channel-levee evolution based on channel trajectories: implications for stratigraphic architecture. *Marine and Petroleum Geology* 28, 716–727. doi:10.1016/j.marpetgeo.2010.05.012.

Van Dijk, W.M., Densmore, A.L., Singh, A., Gupta, S., Sinha, R., Mason, P.J., Joshi, S.K., Nayak, N., Kumar, M., Shekhar, S., Kumar, D., Rai, S.P., 2016. Linking the morphology of fluvial fan systems to aquifer stratigraphy in the Sutlej-Yamuna plain of northwest India. *Journal of Geophysical Research – Earth Surface* 121, 201–222. doi:10.1002/2015JF003720.

Weissmann, G.S., Carle, S.F., Fogg, G.E., 1999. Three-dimensional hydrofacies modeling based on soil surveys and transition probability geostatistics. *Water Resources Research* 35, 1761–1770.

Weissmann, G.S., Hartley, A.J., Scuderi, L.A., Nichols, G.J., Davidson, S.K., Owen, A., Atchley, S.C., Bhattacharjee, P., Chakraborty, T., Ghosh, P., Nordt, L.C., Michel, L., Tabor, N.J., 2013. Prograding distributive fluvial systems — geomorphic models and ancient examples, in: Driese, S.G., Nordt, L.C., McCarthy, P.J. (Eds.), *New Frontiers in Paleopedology and Terrestrial Paleoclimatology*, pp. 131–147. doi:10.2110/sepmsp.104.16.

Willis, B.J., Tang, H., 2010. Three-dimensional connectivity of point-bar deposits. *Journal of Sedimentary Research* 80, 440–454. doi:10.2110/jsr.2010.046.

Wingate, D., Kane, J., Wolinsky, M., Sylvester, Z., 2015. A new approach for conditioning process-based geological models to well data. *Mathematical Geosciences*, 1–27doi:10.1007/s11004-015-9596-8.

Wu, J., Boucher, A., Zhang, T., 2008. A SGeMS code for pattern simulation of continuous and categorical variable: FILTERSIM. *Computational Geosciences* 34, 1863–1876. doi:10.1016/j.cageo.2007.08.008.

Table 1: Observed width dimensions from the present surface (Van Dijk et al., 2016).

Basin	Feature	Width
Sutlej river	channel belt	1600-5000 m
Yamuna river	channel belt	4000-10000 m
Ghaggar	paleochannel	5000-8000 m
Sutlej fan	ridges	650-2300 m
Yamuna fan	ridges	740-1790 m

Table 2: Observed aquifer body thickness distribution statistics from Van Dijk et al. (2016).

Basin	Thickness (m)			Total fraction	
	percentile			aquifer	non-aquifer
	25 th	50 th	75 th		
Sutlej	4.73	7.1	12.1	0.42	0.58
Yamuna	4.1	6.6	10.1	0.43	0.57

Table 3: Modelled aquifer body thickness distribution statistics for various μ values

Basin	μ	5-m interval			f_{μ}	10-m interval			f_{μ}
		Thickness (m)				Thickness (m)			
		percentile				percentile			
		25 th	50 th	75 th		25 th	50 th	75 th	
Sutlej	0.3	5	15	40	0.79	10	20	70	0.77
	0.35	5	15	30	0.68	10	20	60	0.68
	0.4	5	10	25	0.51	10	20	50	0.56
	0.45	5	10	20	0.34	10	20	40	0.42
	0.5	5	10	15	0.21	10	20	40	0.28
	0.55	5	10	15	0.13	10	20	30	0.20
Yamuna	0.3	5	15	35	0.75	10	20	50	0.67
	0.35	5	15	30	0.64	10	20	40	0.57
	0.4	5	10	25	0.48	10	20	40	0.48
	0.45	5	10	20	0.34	10	20	40	0.38
	0.5	5	10	20	0.23	10	20	40	0.31
	0.55	5	10	15	0.15	10	20	40	0.24

Table 4: f_{obs} with distance from the fan apex for the CGWB data and f_{μ} for the 25th, 50th, and 75th percentiles from the model results.

Basin	Distance	f_{obs} fraction	f_{μ}		
			25 th	50 th	75 th
Sutlej	0-50	0.47	0.25	0.53	0.83
	50-100	0.45	0.23	0.35	0.53
	100-150	0.37	0.20	0.30	0.45
	150-200	0.29	0.20	0.30	0.43
	200-250	0.34	0.19	0.30	0.48
Yamuna	0-50	0.41	0.38	0.46	0.58
	50-100	0.38	0.25	0.50	0.78
	100-150	0.42	0.25	0.43	0.65
	150-200	0.29	0.15	0.28	0.43
	200-250	0.26	0.13	0.21	0.36

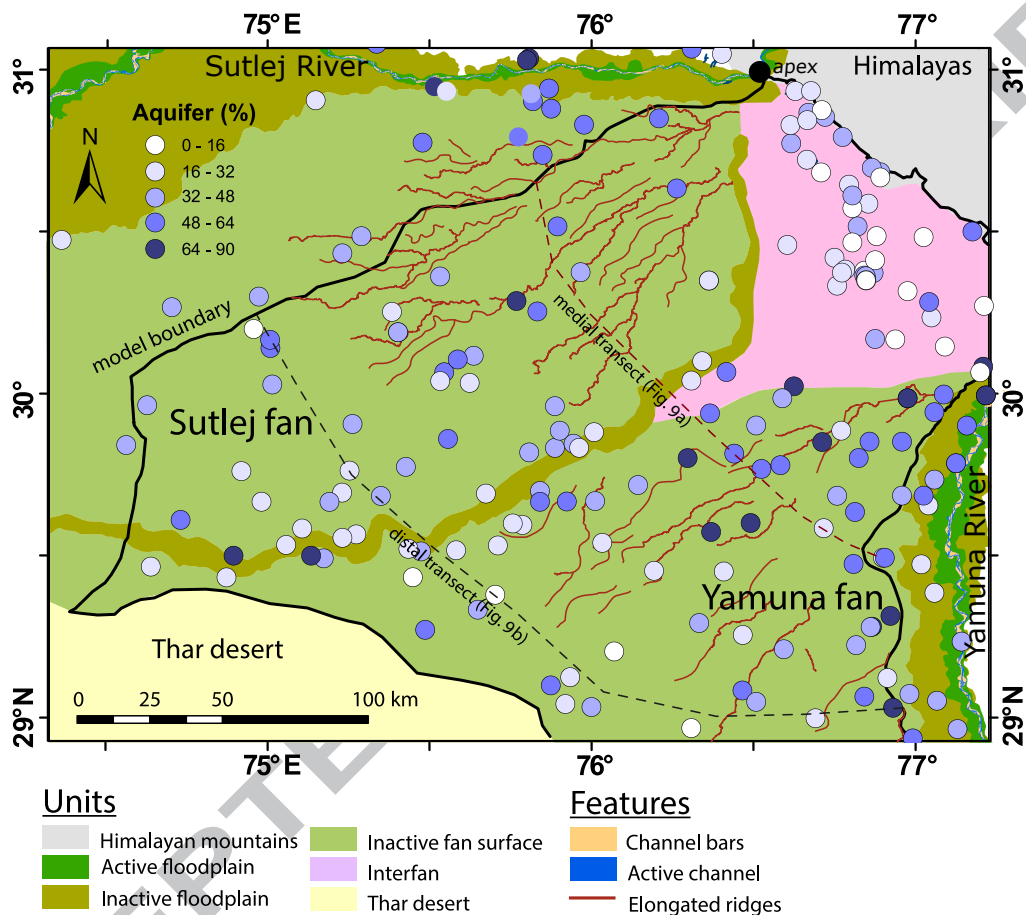


Figure 1: Geomorphological map of the study area (modified after Van Dijk et al., 2016), covering the Sutlej and Yamuna fans and the interfan area between them (pink). Dots show locations of CGWB aquifer-thickness logs (Van Dijk et al., 2016), and colours show bulk percentage of aquifer material in the upper 200 m. The heavy black line indicates the extent of the model space, chosen to include parts of both fans. Dashed lines show the locations of medial (Figure 9a) and distal (Figure 9b) transects.

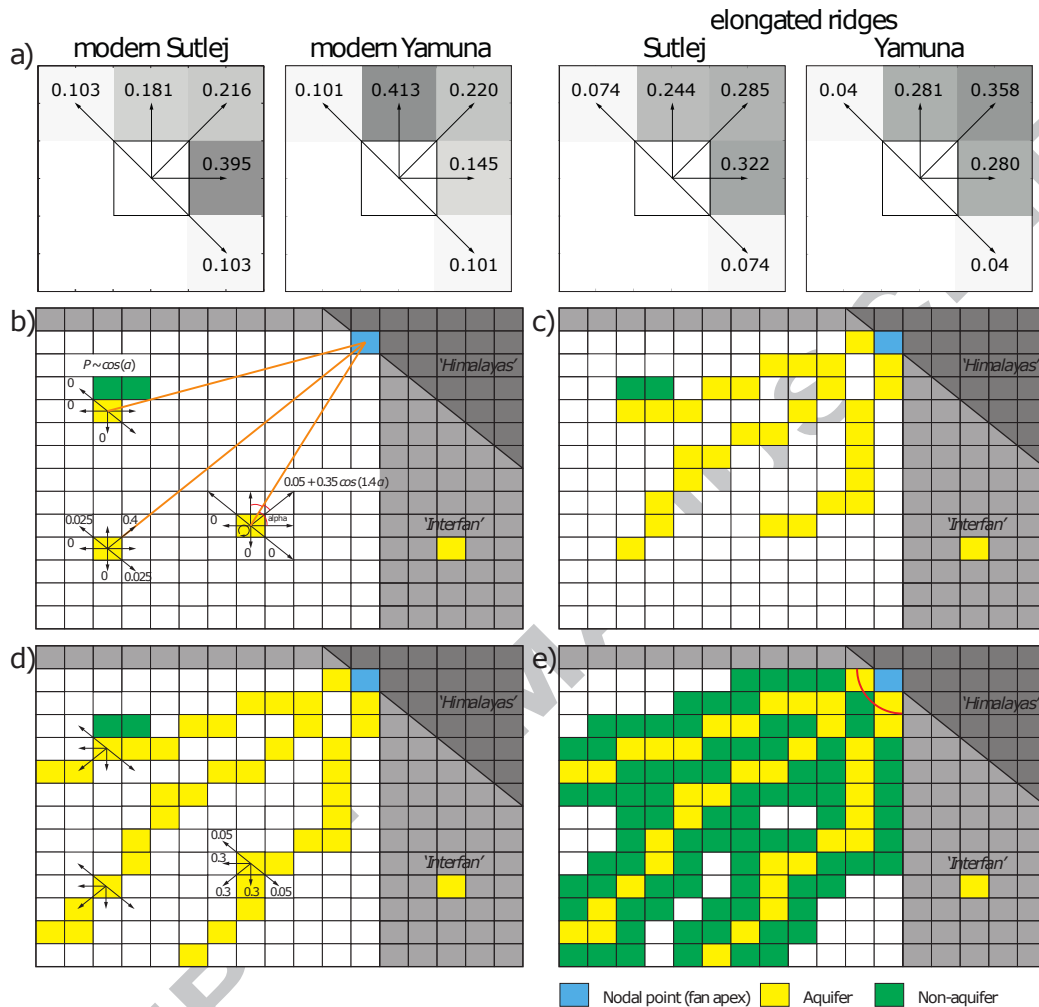


Figure 2: Details of model algorithm and weighted random walk approach as applied in this study. a, directional probabilities derived from the courses of the modern Sutlej and Yamuna channel belts as well as elongate palaeochannel ridges on the Sutlej and Yamuna fans. Numbers and shading show the probabilities that the next upstream channel or ridge cell, toward the fan apex, will occur in one of the eight cardinal directions shown. Probabilities are calculated by the summation of all identified channel or ridge of the adjacent cells for all individual channel or ridge cell, where the probabilities of the cells mirrored to the three cells towards the fan apex are set to zero and probabilities of cells NW and SE direction are divided by two. These probabilities are converted to weights in the random walk used to populate the model with aquifer material. b, schematic showing how the probabilities in (a) are weighted by the angle of the fan apex, and how potential aquifer bodies are routed through the cells around known non-aquifer locations. The probability is modified by a $\cos(\alpha)$ term, in which α is zero towards the fan apex. c, routing of aquifer material upstream toward the fan apex using the weighted probability. d, routing of aquifer material downstream with equal probabilities in the three down-fan directions. e, filling of non-aquifer material in the cells that are laterally adjacent to each aquifer corridor.

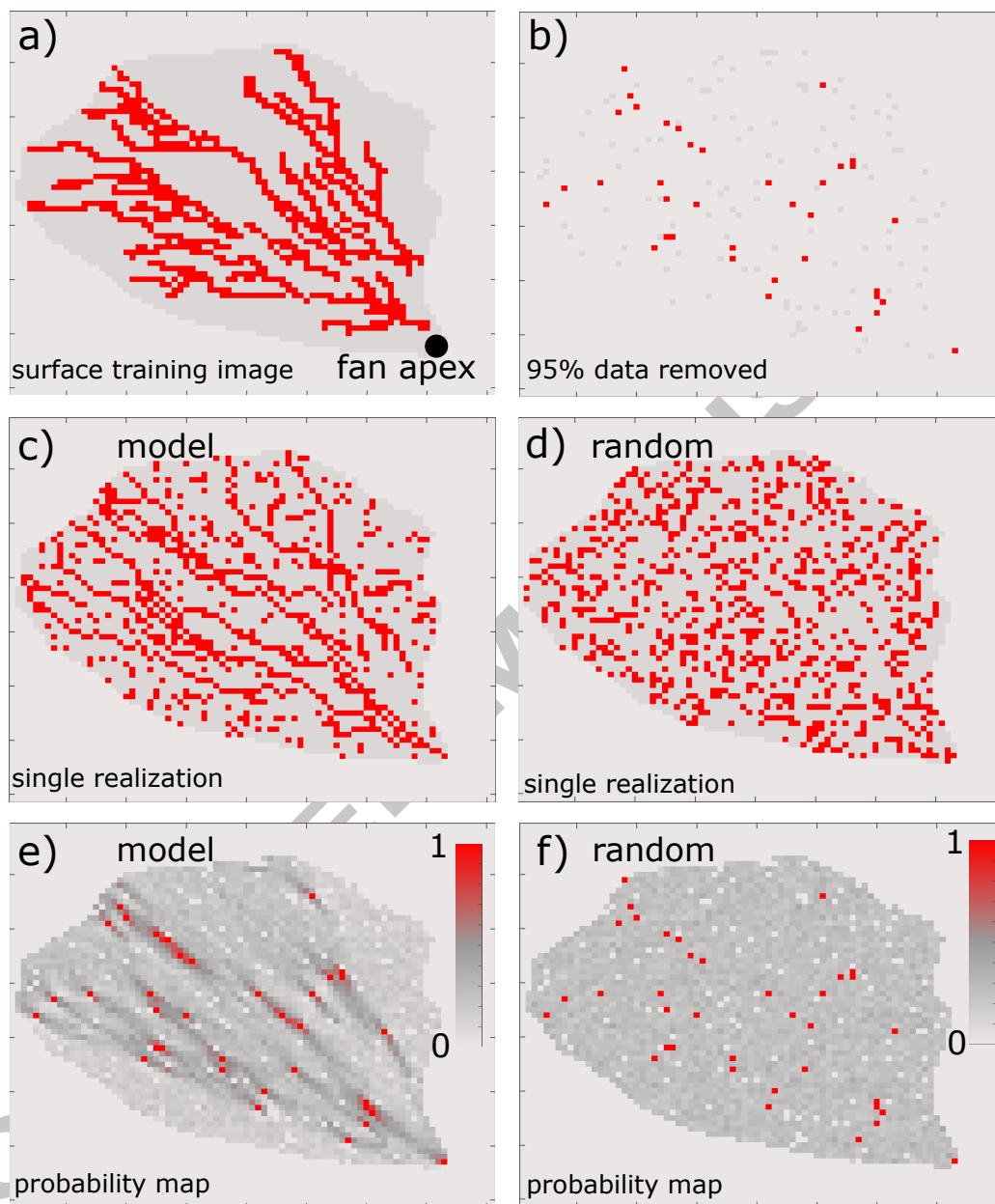


Figure 3: a) Test case of the elongated ridges, used to assemble a quantitative measure of the precision of the model in reconstructing the aquifer pathways. b) In the next step, 95% of the image is removed, leaving 5% of the cells filled with aquifer or non-aquifer. c) Example of a single realization with our model. d) Example of a single realization of random filling of the cells up to 25% with aquifer material. e) Probability map based on 100 realizations from our model. f) Probability map based on 100 realizations from random filling.

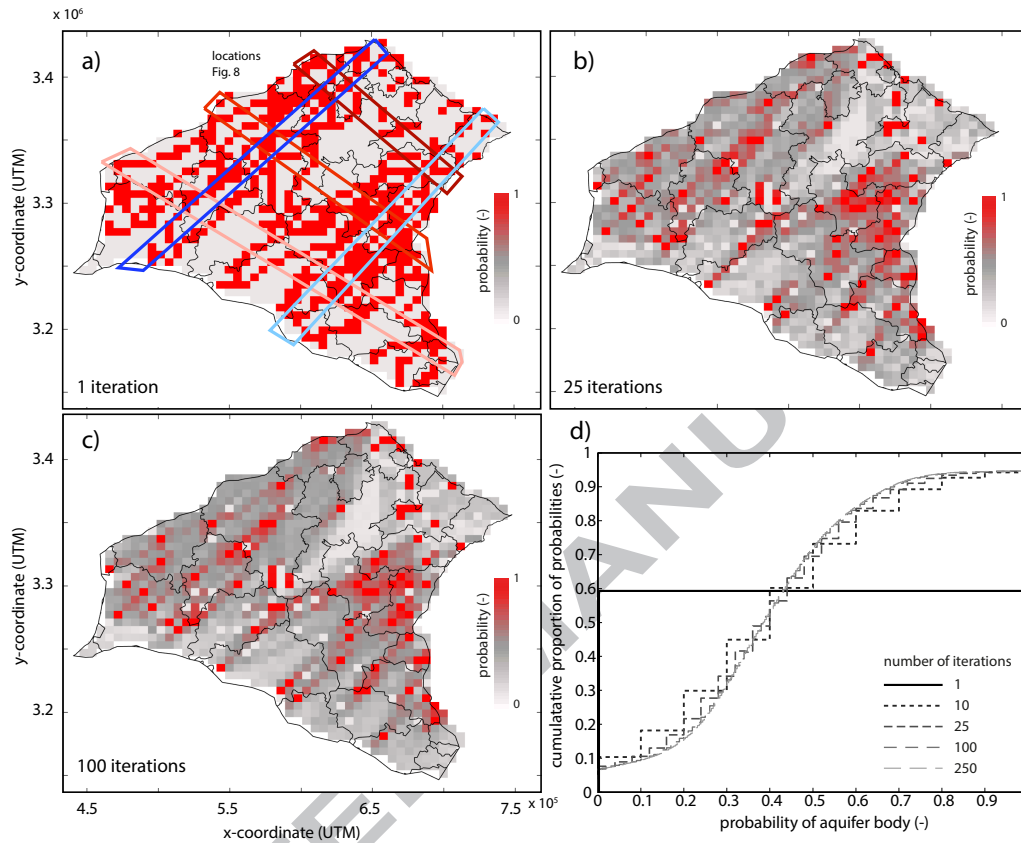


Figure 4: a, results from a single model run for a single depth slice (in this case, 80-90 m below ground level) and a 6 x 6 km grid. In this and subsequent panels, the colour bar shows the probability of finding aquifer material in each cell, and the black polygons indicate district borders for reference. After a single run, the probability is either 1 (aquifer) or 0 (non-aquifer). The colored boxes indicate the locations for the connectivity analysis shown in Figure 8. b, model results after 25 iterations. ‘Known’ cells containing aquifer-thickness logs retain 1 or 0 values, but all other cells contain probabilities in the range [0,1]. c, model results after 100 iterations, showing a somewhat different pattern of probabilities. d, the cumulative distribution of probabilities for all depth slices after different numbers of iterations. Results with 100 and 250 iterations are indistinguishable. Note that the curve does not tend to 0 or 1 because of the presence of known cells with fixed probability values.

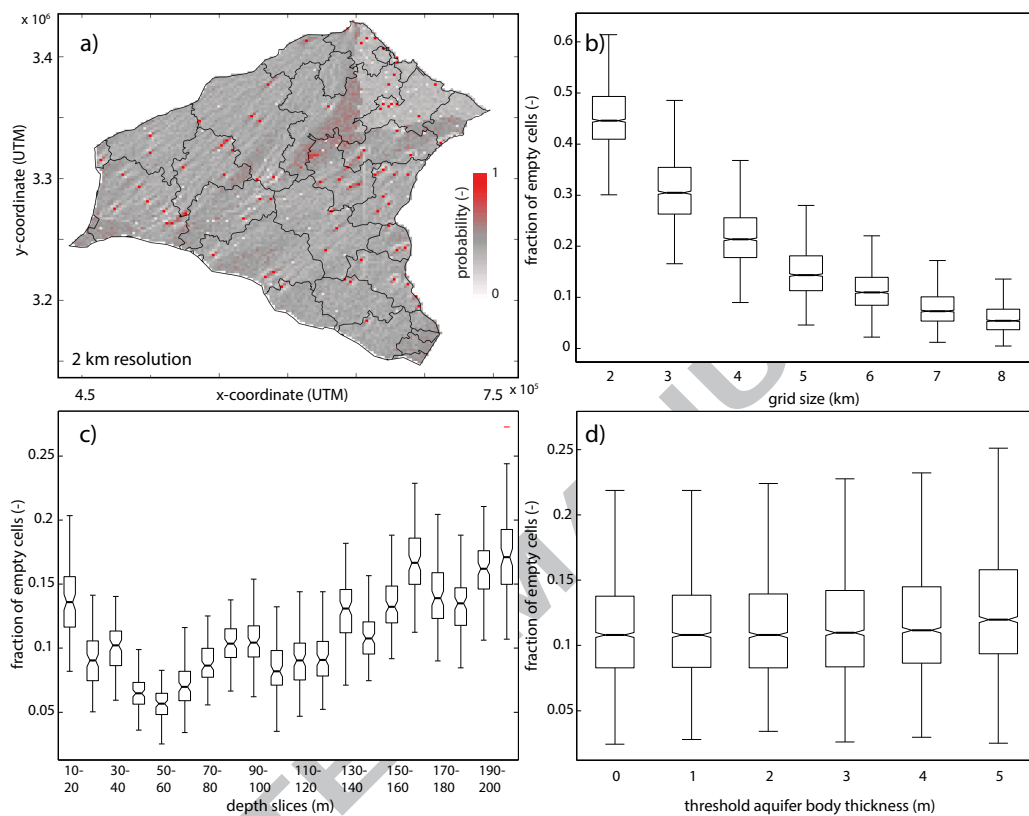


Figure 5: Controls on the fraction of empty cells that must be filled by the model. a, model results using a 2 x 2 km grid and 100 iterations. Compared with Figure 4, probabilities are more distributed, with fewer dominant corridors of high aquifer probability. b, decline in the number of empty cells that must be filled by the model with increasing grid cell size. Boxes show median, 25th and 75th percentiles, and error bars show ± 1 standard deviation for 100 iterations at each cell size. c, variability in the number of empty cells in each 10 m depth slice for 100 iterations. The number of empty cells depends on the aquifer percentage in the input data for each depth slice. d, the fraction of empty cells for runs that ignore aquifer bodies that are less than a given threshold in thickness. This change has no significant effect on the fraction of empty cells.

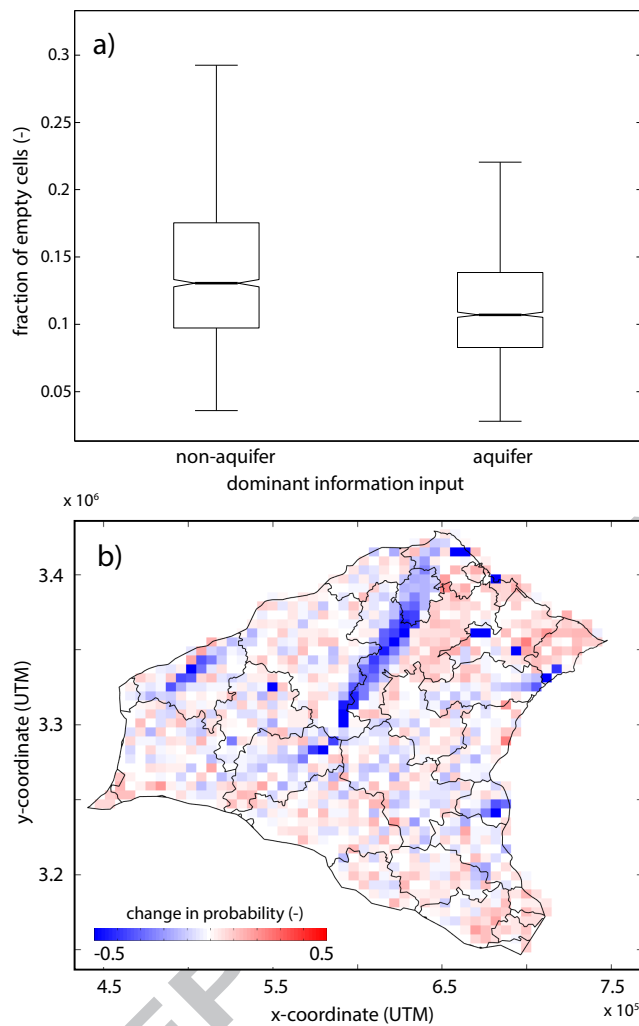


Figure 6: a, the effect of dominance in the input data when multiple well logs occur within a single grid. For runs marked 'aquifer', a cell is classified as aquifer if the majority of at least one input log consists of aquifer material within that depth slice. For runs marked 'non-aquifer', a cell is classified as non-aquifer if the majority of at least one input log consists of non-aquifer material. The cell size is 6 x 6 km, and the model was run for 100 iterations. Note that non-aquifer precedence results in the assignment of a smaller number of aquifer cells, and thus a larger number of empty cells that must be filled randomly. b, spatial pattern of changes in aquifer probability when using aquifer material, rather than non-aquifer material, as the dominant input. The blue colour illustrates the reduction in aquifer probability when the non-aquifer information is dominant. Note that the blue colour follows ³⁹³ of the major aquifer pathways in Figure 4c.

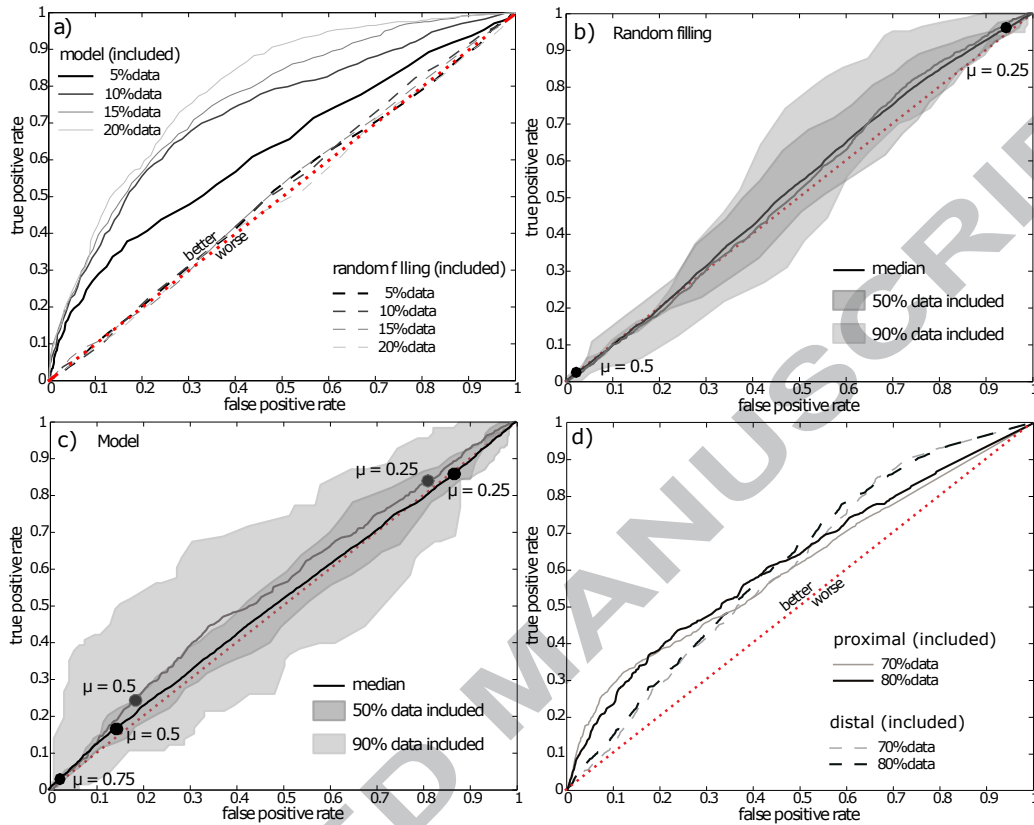


Figure 7: Quantitative characterization of the performance of the model compared to the case of simple random filling. a, ROC curves showing the ability of both model (solid lines) and random filling (dashed lines) to reproduce the positions of elongated ridges on the Sutlej fan surface (the test case). The true positive rate (TPR) shows the proportion of cells that are aquifer material in both the simulated output and the test case, while the false positive rate (FPR) shows the proportion of cells that are aquifer material in the simulation but non-aquifer in the test case. A perfect model would plot in the upper left-hand corner (TPR = 1, FPR = 0). The curves are derived by increasing the probability threshold value from 0 (upper right-hand corner, all aquifer material) to 1 (lower left-hand corner, no aquifers). Different lines show simulations with varying proportions of the input data included, to compare with the model results. The model consistently has a higher TPR-FPR ratio than random filling for all threshold values. b, ROC curves showing the ability of random filling to reproduce a reserved set of input CGWB aquifer-thickness logs. The solid line shows the median output for 50 simulations and the shaded area shows the range between the best and worst simulations. Selected probability thresholds are shown on each curve for reference. c, ROC curves showing the ability of the model to reproduce a reserved set of input logs. Symbols as in panel (b). Note that the region of low FPR, i.e., corresponding to moderate to high values of the probability threshold, would be appropriate for a conservative assessment of the model. In this region, the model has generally a higher TPR-FPR ratio than random filling, especially when more data are included. d, ROC curves showing the ability of the model to reproduce the reserved

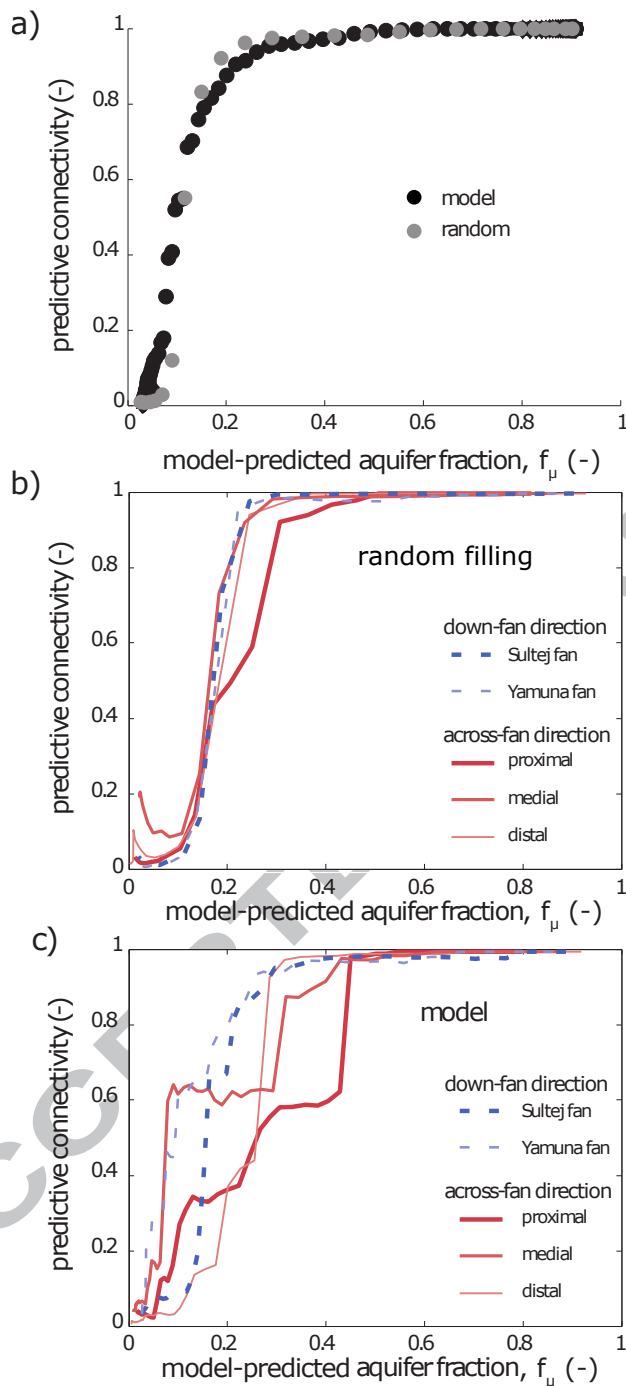


Figure 8: a, smoothed isosurfaces of model potential aquifer bodies for a probability threshold value of 0.45. The aquifer material forms a set of 'ribbon'-shaped bodies that are elongate down-fan, away from the Sultej and Yamuna fan apices. Note that the smoothed isosurfaces are created for visualisation purposes by interpolation of aquifer cells, and are therefore somewhat thicker and wider than the actual data that are used for the analysis. Coloured boxes indicate areas used to evaluate connectivity both parallel to transport (down-fan direction, blue) and normal to transport (across-fan direction, red). b, variation in the connectivity index with increasing f_{μ} , equivalent

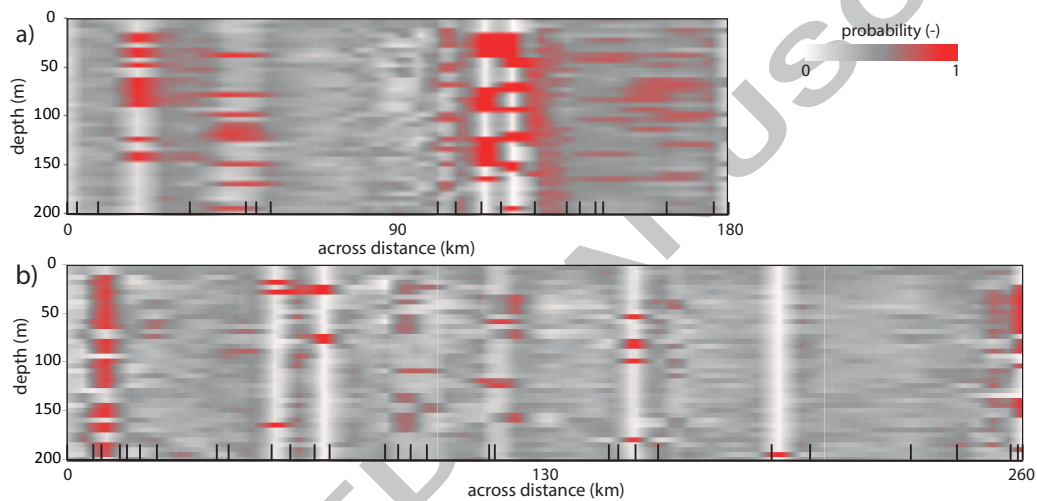


Figure 9: Model probabilities of finding aquifer material along (a) the medial transect and (b) the distal transect, extracted from a model with a grid size of 6 x 6 km, 5 m depth slices, and 100 iterations. The model yields high probabilities at locations near aquifer-thickness logs, whereas areas without borehole information are more likely to be classified as non-aquifer material. Probabilities are overall smaller for the distal transect compared to the medial transect. See Figure 1 for transect locations .

- A new reduced complexity model reproduces simplified fluvial stratigraphy within a fan system
- The model improves forecasting of aquifer body locations compared to random filling
- The model provides testable predictions of the location and distribution of aquifer bodies in the subsurface

ACCEPTED MANUSCRIPT